POLITECNICO DI MILANO

Scuola di Ingegneria Industriale e dell'Informazione

Corso di Laurea Magistrale in
Ingegneria Meccanica

Estimation of Crack Opening Level in Low Cycle Fatigue using Finite Element
Method and Digital Image Correlation

Relatore: Prof. Stefano BERETTA

Correlatore: Prof. Stefano FOLETTI
              Dott. Luca PATRIARCA

Tesi di Laurea di:

Radhakrishna Pai KIZHAKKE PARAMBIL SARVOTHAMA
Matr. 849851

Anno Accademico 2016 - 2017

Ringraziamenti

First of all I would like to thank Prof. Stefano Beretta, Department of Mechanical Engineering in giving me the opportunity to work on this thesis. He was always there to answer my queries and guiding me in the right direction. Without his guidance this thesis would have been impossible. I also thank Prof. Stefano Foletti, in providing an expert support in modeling of material behavior. Whenever I faced problems in the finite element simulations, he would give a proper direction towards solution which immensely helped me in moving forward. I also thank, Dott. Luca Patriarca, without his extreme support running an experimental campaign would be a herculean task. He was always there to supply me with his ideas, which helped me in organizing my work to write a thesis.

I would also like to thank my friends and colleagues at Politecnico di Milano for their encouragement and moral support which made my stay in Italy more enjoyable.

Finally I thank my parents who trusted and supported me throughout my studies here in Politecnico di Milano.

Milano, December 2017 L. M.

Contents

List of Figures

List of Tables

Sommario

La chiusura della crepa è un fenomeno importante da considerare durante l'esecuzione delle valutazioni di vita delle fatiche. La chiusura della crepa nel regime di affaticamento a ciclo basso diventa molto complessa, quindi è stato condotto uno studio sistematico. Le varie tecniche di misurazione utilizzate per misurare la chiusura delle fessure sono state studiate dalla letteratura. Correlazione di immagini digitali (DIC) è una tecnica senza contatto che può essere utilizzata per misurare visivamente i fenomeni di propagazione della crepa con l'aiuto della fotocamera e di un software DIC. Ci sono alcuni metodi di conformità che possono essere utilizzati per stimare il livello di apertura della crepa da Crack Opening Displacement (CKO) rispetto alla curva di isteresi Stress. Ma c'è un requisito di un metodo semplice e robusto che può essere utilizzato per misurare il livello di apertura dal COD contro la curva Stress. Nella fase iniziale della tesi, i parametri dei modelli di materiale Chaboche dell'asse dell'acciaio ferroviario A4T e KSA30 sono identificati dai dati dell'esperimento di fatica a basso ciclo. Questi parametri vengono utilizzati per simulare la propagazione delle cricche nel software Finite Element ABAQUS. Con l'aiuto di risultati di Finite Element, viene sviluppato un nuovo metodo semplice e robusto utilizzato nei risultati DIC per misurare il livello di apertura della crepa. Infine i livelli di apertura sperimentali vengono confrontati con i livelli di apertura degli elementi finiti.

Parole chiave: Ciclo di bassa fatica, Apertura della crepa, Chiusura della crepa, Modello di materiale di Chaboche,

Abstract

Crack closure is an important phenomena to consider when performing fatigue life assessments. The crack closure in low cycle fatigue regime becomes very complex, therefore a systematic study has been conducted. Various measurement techniques which was used to measure crack closure has been studied from literature. Digital Image Correlation (DIC) is a non-contact technique which can used to measure the crack propagation phenomena visually with the help of camera and a DIC software. There are some compliance methods which can be used to estimate the opening level of the crack from Crack Opening Displacement (COD) versus Stress hysteresis curve. But there is a requirement of a simple and robust method which can be used to measure opening level from COD versus Stress curve. In the initial phase of the thesis, Chaboche material model parameters of A4T and KSA30 railway axle steel is identified from the data of Low cycle fatigue experiment. This parameters are used to simulate crack propagation in Finite Element software ABAQUS. With the help of Finite Element results, a new simple and robust method is developed which is used in DIC results to measure crack opening level. Finally the experimental opening levels are compared with finite element opening levels.

Keywords: Low Cycle Fatigue, Crack opening, Crack closure, Chaboche Material Model

Chapter 1

Literature Review

1.1 Fatigue Crack Growth in Low Cycle Fatigue

Mechanical components which are subjected to high amplitude fatigue loading at different temperatures are designed based on Low Cycle Fatigue (LCF). In LCF regime, it is not possible to apply procedure based on ΔK, since the size of the yield zone in front of crack tip becomes large compared to characteristic dimensions of the component, which violates the Linear Elastic Fracture Mechanics (LEFM) assumptions [8]. To describe crack propagation in LCF condition two different approaches are proposed. The first one is based on Elastic-Plastic Fracture Mechanics (EPFM): according to this approach, the stress intensity factor range ΔK, is replaced in the Paris equation by Cyclic J-Integral ΔJ. The ΔJ is a measure, which is capable of characterizing the state at the crack tip even if the plastic zone is not confined to a very small region compared to characteristic dimensions. Second one is based on Phenomenological model, in which crack propagation under LCF conditions are described as a function of the applied plastic range.

1.2 Cyclic J-integral models

The J contour integral was presented in 1968 by Rice [9]. He represented the elastic-plastic nonlinear constitutive behavior to a non-linear elastic behavior. Rice then shows that the non-linear energy release rate J, can be written as a path independent line integral as per equation (1.1),

$$J = \int_{\Gamma}(wdy - T_i\frac{\partial u_i}{\partial x}ds) \tag{1.1}$$

- w is the strain energy density;

- T_i are the components of the traction vector, allow to follow the crack when it oversteps the limits of the analyzed region;

- u_i are the displacement vector components;

- ds is the length increment along the contour Γ as shown in Figure 1.1;

1
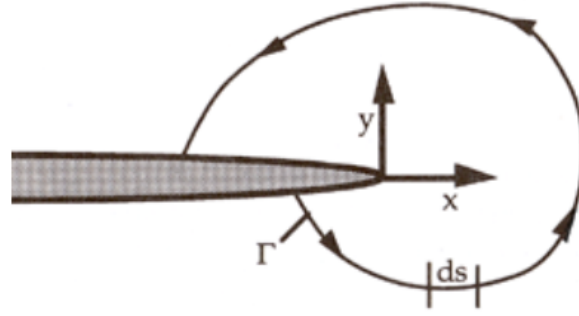
Figure 1.1: Contour for J integral

The J integral is only path independent for linear-elastic, nonlinear-elastic material and materials which follows deformation plasticity theory. In case of fatigue, when unloading occurs in an elastic-plastic material, deformation plasticity theory no longer describe the actual behavior of the material. Thus high path dependent values result in the situation of unloading and are therefore questionable to use in the fatigue situation. Despite the loss of generality, several researchers have tried to use the ΔJ for correlating the crack growth rate, with different degrees of success. Dowling [10] replaced the stress intensity factor range ΔK of Paris equation with ΔJ.

According to Dowling [11], ΔJ is calculated by replacing in the analytical formulation of J with cyclic stresses and strain ranges. This means that ΔJ is calculated by replacing the monotonic Ramberg-Osgood Equation (1.2) with cyclic stress and strain range neglecting the unloading part of the curve.

$$\varepsilon = \varepsilon_{el} + \varepsilon_{pl} = \frac{\sigma}{E} + \left(\frac{\sigma}{K_i}\right)^{1/n_i} \tag{1.2}$$

Dowling's formulation also assumed that the cyclic J-Integral is the sum of an elastic and a plastic component. Starting from the works of Shih [16] and Shih and Hutchinson [17], Dowling [18] demonstrated that, the elastic part of ΔJ is a function of applied stress range, $\Delta\sigma$, whereas the plastic component ΔJ is a function of the plastic strain range $\Delta\varepsilon_p$. The general formulation of ΔJ is reported in Equation (1.3).The elastic part of ΔJ not only depends on the applied stress range, but also on constant Y which takes into account the geometry of the cracked component and on crack length a. Also, elastic component is a function of plane stress or plane strain. For plane stress $E' = E$ and for plane strain $E' = E/(1 - \nu_2)$.

$$\Delta J = \Delta J_{el} + \Delta J_{pl} = Y^2 \frac{\Delta\sigma^2}{E'}\pi a + g(n_i)\Delta\varepsilon_p \pi a \tag{1.3}$$

The plastic component of ΔJ depends on a function, $g(n_i)$, which is a function of exponent of cyclic stress/strain curve n_i. The most used formulation of $g(n_i)$ is shown in Equation (1.4) (Source [18]). This correction factor also depends on the whether the loading condition is plane stress or plane strain at the crack tip.

$$g(n_i) = \begin{cases} \frac{1}{\sqrt{n_i}} & \text{plane stress} \\ \frac{3}{4\sqrt{n_i}} & \text{plane strain} \end{cases} \tag{1.4}$$

In literature, there are several ΔJ based models for describing crack propagation in LCF. Harkegard applied this kind of model to assess the life of the specimen tested at $R_\varepsilon = -1$ in LCF. In order to have conservative estimation, Harkegard considered the $\frac{da}{dN}$ vs ΔJ curve obtained at $R_\varepsilon = -1$.
Harkegards formula for ΔJ is shown in (1.5)

$$\Delta J = Y^2 \pi c \Delta\sigma(\Delta\varepsilon_{el} + 2\Delta\varepsilon_{pl}) \tag{1.5}$$

Crack closure effects were implemented in ΔJ calculations by McClung and Sehitoglu [14, 22] together with Vormwald and Seeger [20, 23]. The reduction of cyclic J-Integral range was implemented by lessening stress and plastic strain ranges, considering only the portion of the load cycle in which the crack stays open. Then, Vormwald and Seeger formulated the following definition of ΔJ based on the assumption that the opening and closing phenomena happen at the same strain level [20]:

$$\Delta J_{eff} = c[1.24\frac{\Delta\sigma^2_{eff}}{E} + \frac{1.02}{\sqrt{n'}}\Delta\sigma_{eff}\Delta\varepsilon_{pl,eff}] \tag{1.6}$$

Also, McClung and Sehitoglu proposed the following equation of cyclic J-integral assuming that opening and closing of crack occur at same stress level [14]:

$$\Delta J_{eff} = 1.25\pi c[\frac{\Delta\sigma^2_{eff}}{E} + \frac{h(n')}{\sqrt{\pi}}\Delta\sigma_{eff}\Delta\varepsilon_{pl,eff}] \tag{1.7}$$

$$h(n') = 3.85(1-n')\sqrt{1/n'} + \pi n' \tag{1.8}$$

1.3 Phenomenological models

Phenomenological models are based on the assumption that in LCF regime the crack growth rate is a function of the applied plastic range $\Delta\varepsilon_p$. The commonly used model is the one introduced by Tomkins [24]. Tomkins correlated crack growth to the plastic strain amplitude by exponential law as shown in Equation [(1.9)]

$$a = a_i e^{k_g N} \tag{1.9}$$

Crack growth rate is defined by differentiating the above equation by N and it is obtained Equation [(1.10)] that crack growth rate is directly proportional to the crack length a and k_g.

$$\frac{da}{dN} = k_{g0}\varepsilon^d_{ap}a \tag{1.10}$$

k_g is defined as a function of two material parameters, k_{g0} and d.

$$k_g = k_{g0}\varepsilon^d_{a,p} \tag{1.11}$$

The number of cycles to failure can be obtained by integrating the Equation [(1.12)]

$$\frac{da}{a} = k_{g0}\varepsilon_{a,p}^d dN \tag{1.12}$$

to obtain Equation [(1.13)]:

$$N_f = \frac{1}{k_{g0}\varepsilon_{a,p}^d} ln(\frac{a_{fin}}{a_0}) \tag{1.13}$$

N_f can be calculated using Coffin-Manson law, to obtain:

$$N_f = \frac{1}{2}(\frac{\varepsilon_{a,p}}{\varepsilon_{f'}})^{1/c} \tag{1.14}$$

This procedure allows to define the material parameters:

$$d = -\frac{1}{c} \tag{1.15}$$

$$k_{g0} = 2(\varepsilon_{f'})^{1/c} ln(\frac{a_{fin}}{a_0}) \tag{1.16}$$

Rabbolini et.al [25] used such a model for assessing the accuracy in life prediction. It was found out that at high strain ranges, the model describes crack propagation with high accuracy. As strain ranges becomes lower less accuracy of the result is seen. This is because the model considers only the plastic component of the applied strain range.

1.4   Crack Closure

In the early 1970's, Elber reported the phenomena of Crack Closure[1]. It is a phenomenon in fatigue loading,in which the fracture surfaces comes into contact even during cyclic tensile loading. This means that the crack opens only above a particular stress-level called Opening level. He attributed the occurrence of this fracture surface contact to the plastic deformation in the wake of a growing crack. The main consequence of this process is that it provides a longer life for fatigue-loaded material than expected, by slowing the crack growth rate. Elber proposed to use ΔK_{eff} as crack driving parameter in place of considering the nominal stress intensity factor ΔK_{nom}.

$$\Delta K_{nom} = \Delta K_{max} - \Delta K_{min} \tag{1.17}$$

$$\Delta K_{eff} = \Delta K_{max} - \Delta K_{closure} \tag{1.18}$$

where $\Delta K_{closure}$ is the stress intensity factor at which crack opens.

The use of ΔK_{eff} eliminates the load ratio dependence in crack propagation and all fatigue crack growth curve $log(\frac{da}{dN})$ vs ΔK coincide to a common line. Not only there are large number of studies supporting the importance of crack closure,
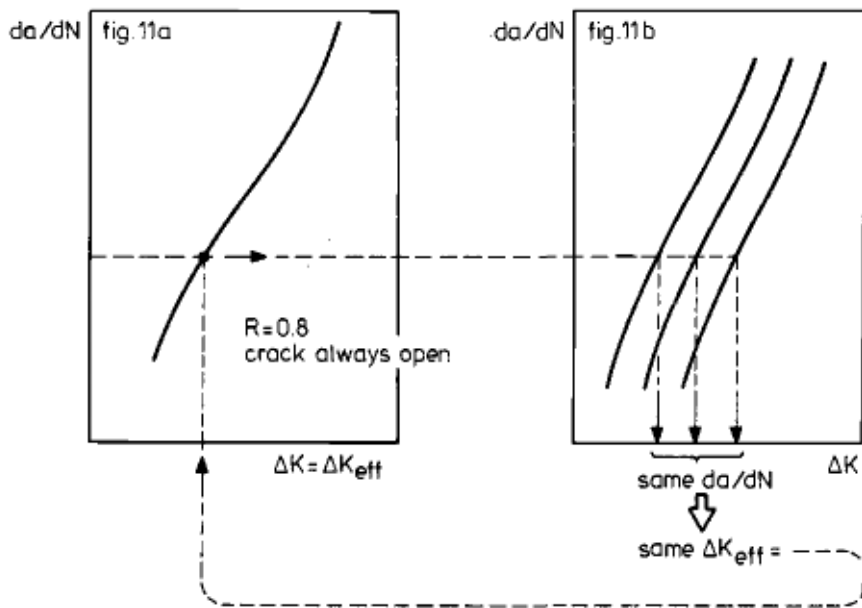
Figure 1.2: Derivation of K_{eff} from da/dN, method adopted by Zhang et al. source[7]

but also there are several papers that noticed doubts on this concept, for example, Refs.[4,5,6]. Elber [1,2] also observed a change in compliance during loading part of the hysteresis loop and concluded that this is due to change in crack length due to the closure of crack faces behind the crack tip, even though the global load is positive.

The difference between crack propagation data at different R-values gives the crack closure level. By enforcing the crack growth rate in the actual test to be same as in the crack closure free experiment one can estimate the crack closure level from fatigue crack growth rate data. This approach was adopted by Zhang et al.[7]. He assumed that cracks remain fully open at R=0.8. The results were adopted as a calibration to obtain ΔK_{eff} at lower R ratios. The method is shown in Figure 1.2 This definition eliminates the need for accurate crack closure measurements during the actual test, but requires a fatigue crack growth rate experiment where no crack closure is present.

Crack closure effects may have several different origins. The origin to this may be due to corrosive environment that causes the newly created crack faces to oxidize/corrode. This oxide layer can be seen as the wedge inserted into the crack. Hence, there is a reduction in effective stress intensity factor range. This type of crack closure mechanism is called Oxide Induced Crack Closure. Another cause is during the crack growth, the crack-tip plastic deformation leaves a wake of deformed material behind the crack tip. This wake has residual compressive stress and it will close the crack when the stress is below a certain level. This type of crack closure is called Plasticity Induced Crack Closure, which is the main focus of this thesis. A third type may occur if a Mode I growing fatigue crack is subjected to a Mode II overload, Due to heterogeneity in micro structure, microscopic roughness of fatigue fracture surfaces is present. As a result, mismatch can occur between

the upper and lower crack faces during displacement in mode 2 loading. These mismatch wedges open the crack, resulting in crack closure. Due to the relative displacement in the crack plane retardation effects occur that may affect the crack growth rate several millimeters ahead.

The majority of conducted research on crack closure is focused on High Cycle Fatigue where Linear Elastic Fracture Mechanics is applied, which is natural since the incorporation of closure level into the fatigue crack growth law is straightforward by use of the stress intensity factor range. Under Low Cycle Fatigue conditions,no parameter exist which is theoretically justified and simple engineering type. This is probably one of the reasons for less amount of research work conducted in the LCF compared to the HCF.

1.4.1 Crack Closure Measuring Techniques

Several researchers use the compliance based methods to measure the crack closure level during crack propagation in LCF conditions. For LEFM, majority of researcher places a strain-gage close to the crack tip during load cycles. This method is not possible to use under LCF due to high plastic deformation in the vicinity of the crack tip.
In 1976, Dowling and Begley [11] conducted the LCF test on compact tension specimen made of A533B steel. Shallow threaded holes were made on the both sides of the crack plane as shown in Figure 1.3. Knife edges were attached in order to measure deflection along the crack line with a clip-gage. The load applied was deflection control to a sloping line with negative load ratio ($0 \leq R \leq 1$). As the crack extends, the clip gage was moved in order to be as close to crack tip as possible. The side clip-gage displacement is plotted versus the load-line displacement and the non-linearity point is used as the crack closure level. This closure level is compared with the closure level estimated directly from the load displacement data taken from the load line. No significant difference was observed and the crack closure level from the clip-gage at the load line was used as in Figure 1.4. They stated that this is just a first order estimation of effect of crack closure and there is no significance in going into its details.

El-Haddad and Mukherjee [29], Jolles[31] , Tanaka et al. [30] and several others all used the same method (load line displacement versus applied load) as Dowling and Begley for estimating the crack opening and closure level and the crack length is almost always measured by a visual system. The load line displacement versus applied load presented by Jolles is shown in Figure

A systematic experimental study of the crack closure behaviour in LCF has not been published yet, even though some measurements have been conducted. Iyyer and Dowling [19] conduct fully reversed strain controlled LCF tests on smooth specimen axial specimens and measure the crack opening and closing levels. The trends show that the crack opening level decrease with increase in strain range, with closure level decreasing more than the opening level. Closure level is negative, which means crack is still open at negative global loads when plastic strains are present. Due to limitations in the experimental equipments, the closure measurements are not sensitive as desired.

In 1988 McClung and Sehitoglu [14] conducted experiment to determine the
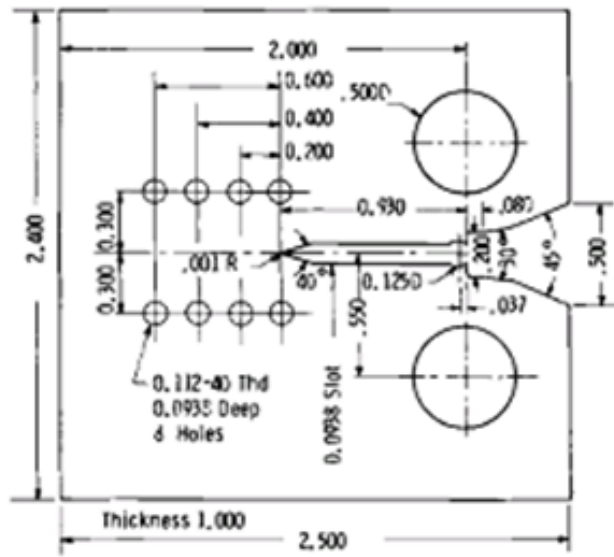
Figure 1.3: Specimen for estimation of Cyclic J Integral. source[11]

$$\Delta J = \frac{2 \text{ (Hatched Area)}}{Bb}$$
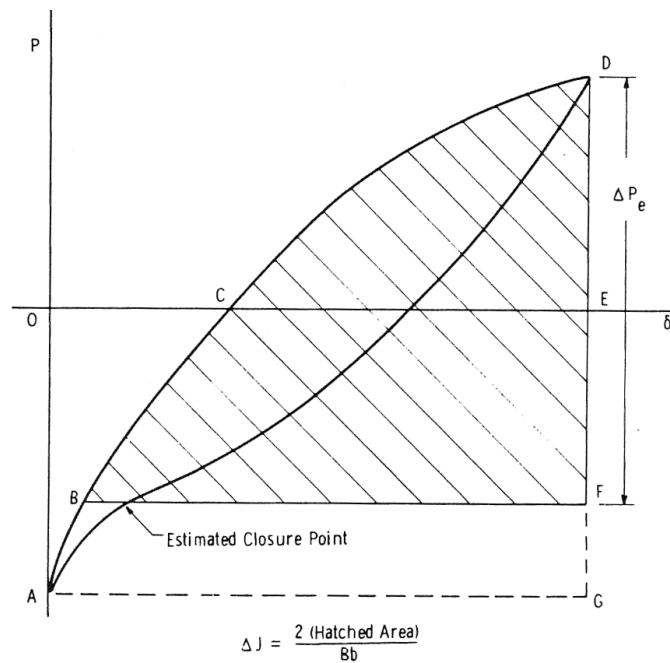
Figure 1.4: Estimation of Cyclic J Integral. source[11]
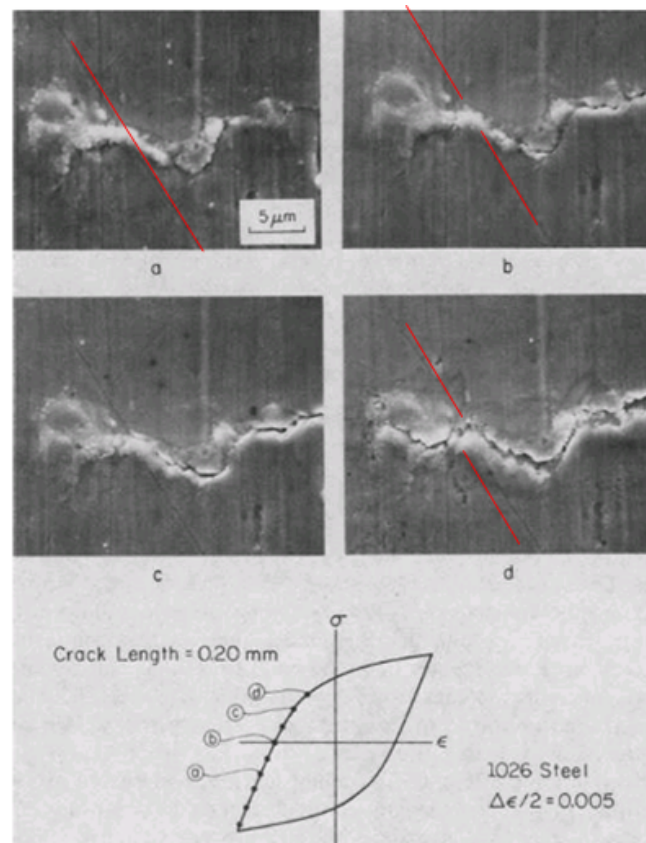
Figure 1.5: Crack Opening Level Measurement using acetate replicas and SEM[14]

closure behavior of small cracks under high strain fatigue loading. The specimen used was notched axial specimen with 50 μm made of 1026 hot rolled SAE steel. The authors used two types of loading: constant amplitude with load ratio of -0.25 for strain amplitude of 0.001 mm/mm and load ratio -1 for strain amplitude of 0.2% - 0.7%. Followed by variable amplitude loading with load ratio of -1. Opening and closing behavior of the cracks at the surface was studied with two stage replica process. Acetate replicas were taken during the test and then at a later time selected replicas were processed for inspection with Scanning Electron Microscopy. This procedure produced a series of snap-shot of the cracks as shown in Figure 1.5, as it gradually opened across entire gage length. There is a polishing mark (shown in red) aligned at 45 degrees to the specimen axis. It would be continous when closed. It would be offset when the crack is open and this offset distance is directly proportional to the crack opening displacement (CTOD). The normalized crack opening level is observed to decrease with increasing strain amplitude for constant amplitude histories. The crack closing level is also observed to decrease with strain amplitude and becomes significantly lower than the opening levels at high strain. Figure 1.6 shows the crack opening dependence with maximum stress.

Vormwald and Seeger [20] further conducted experiments to explore the consequences of short crack closure under variable amplitude loading. They conducted experiments of Fe460 and Al 5086 materials for different load ratios of $R = 0.7, 0.4, 0, -0.4, -1.0$. The load applied was same as that used by Dowling.
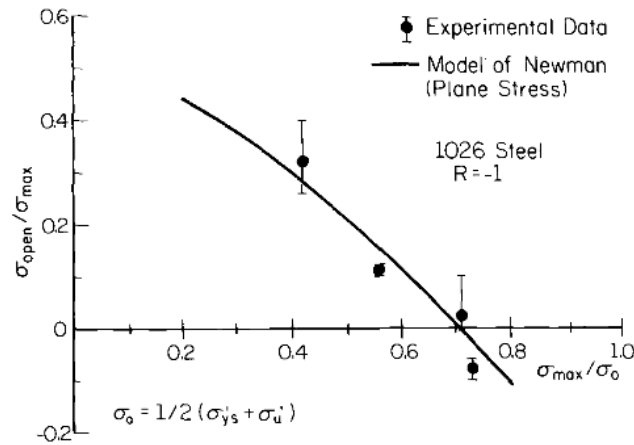
Figure 1.6: Experimental Vs Analytical (NewMann analysis) . source[14]
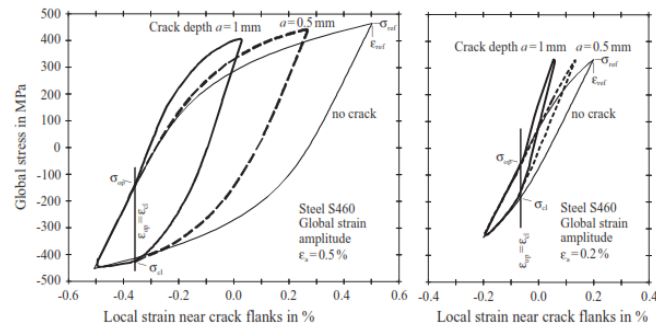
Figure 1.7: Crack opening and closure of semi-circular surface cracks. source[20]

Crack closure was measured at three values of crack length using a traveling strain gage. The authors were able to successfully measure the opening and closing level and came up with a new finding that opening and closing level occurs at same value of strain as shown in Figure 1.7 , which is different from high cycle fatigue case where opening and closing occurs at the same stress.

R. Pippan and W. Grosinger[21] used Scanning electron microscopy to create take images of a cycle at different time intervals to measure crack opening and closing level. The SEM was synchronous to the loading. The SEM micrograph of closing crack can be seen in Figure

1.4.2 Non-contact Crack Closure Measuring Techniques

There are varieties of experimental measurements based on extensometer or strain gages to measure crack closure. The advancement in computer vision opened a way to the introduction and development of non-contact techniques like Digital Image Correlation (DIC). In this section, it is explained the overview of DIC and it's application in fatigue crack growth.
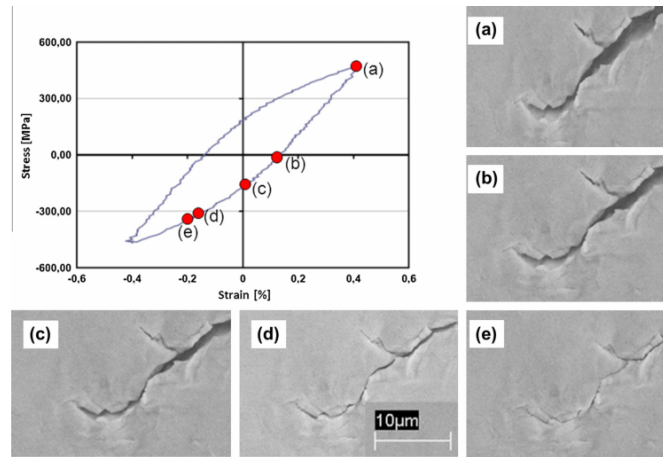
Figure 1.8: SEM Micrograph of crack closure.source [20]
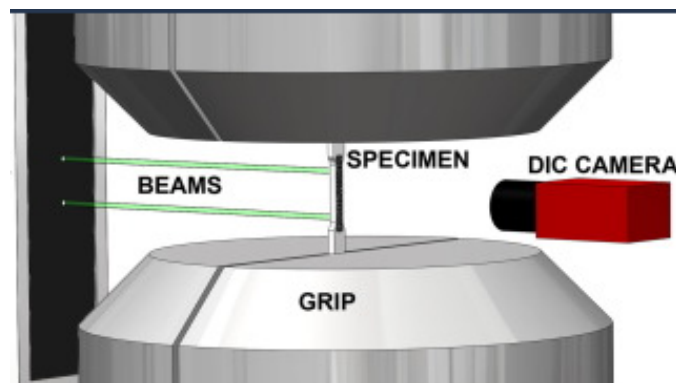
Figure 1.9: Schematic of DIC Experimental Setup

Digital Image Correlation

DIC was developed at the University of South Carolina in the early 1980s [32-35], with the idea of measuring full-field in-plane displacement gradients of a strained body. The main principle used in DIC is that displacements can be calculated by comparing the position of features present in two images of a target surface.

The experimental setup schematic is shown in Figure 1.9. The camera is focused on the region of the specimen. A parallel beam of light illuminates the area. The specimen is gripped to the tensile test machine. The camera captures the sequence of digital pictures. The number of pictures vary as per the cycling frequency. Lower the frequency of loading more number of pictures will be captured per cycle. The further analysis is done by DIC software.

The pixel positions of a set of digital pictures are tracked by DIC software. The first picture of the set is usually taken at zero load. This is called reference or undeformed image, while the other images is acquired from video recorded when the body is externally loaded and are called as deformed images. In theory,it is impossible to uniquely define the relative position of each pixel in the reference image with the deformed image. The correlation algorithm tracks the change in position of a small group of pixels called subsets. Figure 1.10 shows an example of how the correlation algorithm works.
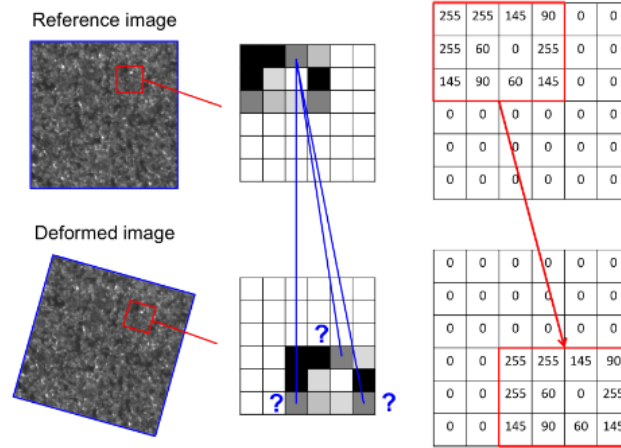
Figure 1.10: Subset tracking illustration [36]

The critical parameter in the correlation algorithm is the size of the subset. In order to achieve accurate results, the dimension of the subset should be as small as possible, but the smaller size should also guarantee an accurate identification of the subset in the deformed image. This mainly depends on the dimension of the features present on the measurement surface.

The target surface should be prepared carefully. Different techniques are adopted for making the pattern. Random speckle pattern is realized on the surface with black paint using airbrush. This random speckle pattern corresponds to a group of pixels on the gray scale (from 0, black, to 255,white). The images are acquired using monochrome digital camera. Later in the thesis it can be seen that this type of speckle pattern gives a satisfactory results in the measurement of displacement field around crack-tip even at high magnification.

In this thesis, the main focus is on In-Situ DIC measurement.The images are acquired during the experiment, when the specimen is mounted in the load frame, and the displacement fields can be measured in real time. This type of measurement is used in fatigue loading, since we can analyze the evolution of the displacement field around a crack during a fatigue cycle, allowing the measurement of crack opening and closing levels. In the next section, the application of In-Situ DIC to fatigue is discussed.

1.4.3   Crack Closure Measurements using DIC

Some researchers have tried to extensively use DIC for Low Cycle Fatigue crack closure measurements. Rabbolini et. al [26] used DIC experiment to measure closure levels of a LCF specimen. Measurement of opening level were performed from COD and local strain cycles. Experiments were conducted at $\varepsilon_a = 0.25\%(R = 0.5; -1)$ and $\varepsilon_a = 0.35\%(R = -1)$. The samples were having 0.4 mm radius semi-circular defect from EDM. All the samples were precracked using Compression Precrack Constant Amplitude to remove nucleation time. Two methods were used to measure opening level as follows and is illustrated in Figure 1.11:

- Virtual Crack Mouth Opening Displacement: Series of digital extensometer were
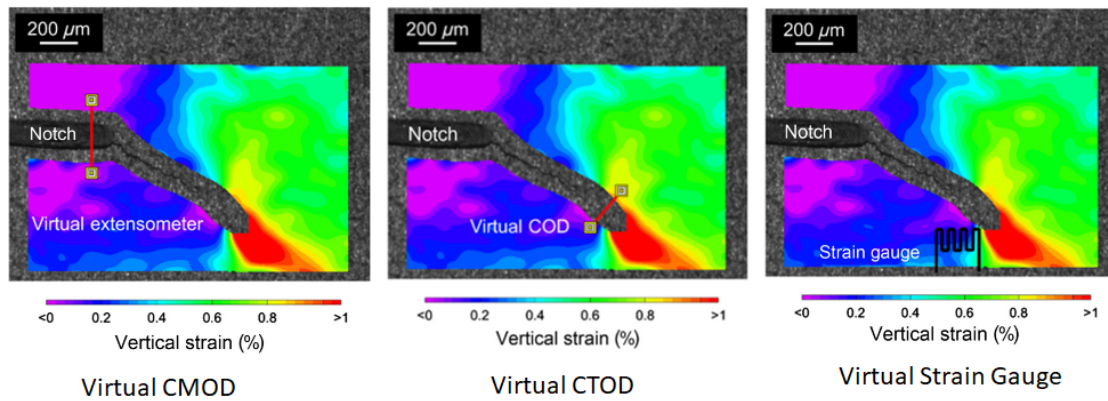
Figure 1.11: Different DIC measuring techniques [26]

placed across the flanks of the EDM notch. The closing and opening levels were calculated using offset procedure.

- Virtual Crack-Tip Opening Displacement: A pair of two-point digital extensometer were positioned across the crack flanks at 100 μm and 200 μm behind the crack tip.

- Virtual Strain Gage: A virtual strain gage is placed between cyclic plastic zone and the notch. From this, it was proved that opening and closing level occurs at same level of strain. Opening level doesn't depend on the distance from the crack tip.

He has also performed another investigation on line pipe steel [26] to measure crack closure using DIC. Same specimen geometry was used with compression pre-cracking constant amplitude technique. The experiment was performed till the crack length of 2mm is reached. Virtual strain gage was used. This experiment was repeated on Large Scale Specimen, but the crack opening and closing levels are higher due to plane stress condition. Crack front was elliptical rather than circular. This technique was able to measure opening level, but it loses its accuracy during the unloading part of the hysteresis loop.

1.4.4 Numerical Simulation of Plasticity Induced Crack Closure

In LCF regime, it is expected plasticity induced crack closure to be the dominating crack closure mechanism. No systematic study has been conducted and still very few papers are published regarding the PICC, FEM, LCF.

Element Size

The element size along the crack path is important. Many elements must be used sufficiently to resolve the high stress gradients in front of the crack tip. The element size determines the simulated crack growth rate. The first investigation of crack closure by finite element was conducted by Newman[12]. He showed that a
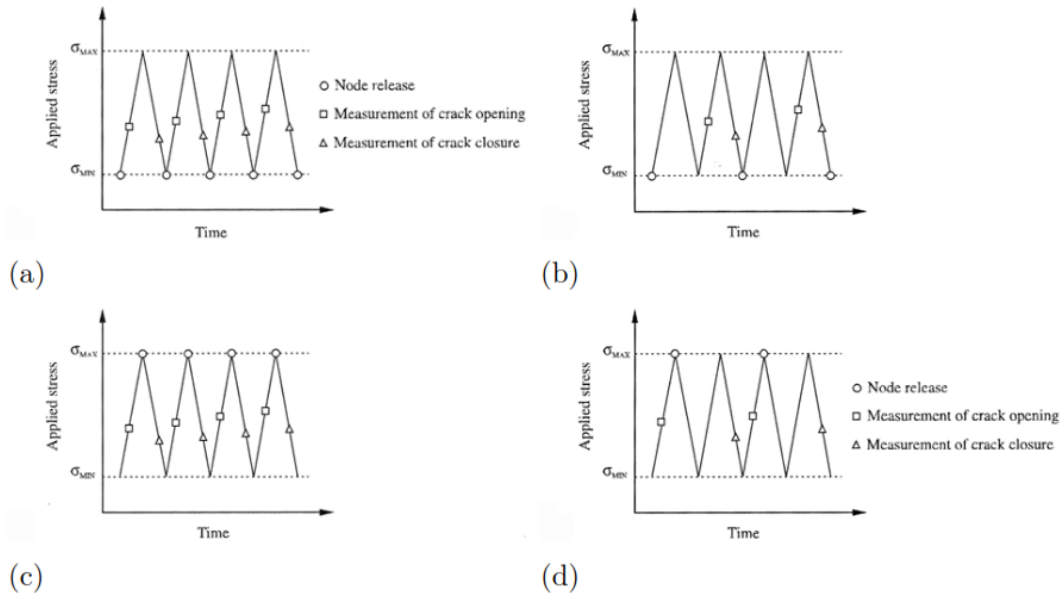
Figure 1.12: Different commonly used node release schemes [13]

much finer mesh is needed in order to obtain convergence when low nominal stress levels are used as compared to high stress levels. So the element size requirement can be relaxed when applying higher loads.

Node Release Scheme

One of the main disadvantage of simulating fatigue crack growth in finite element method is there would be relatively large discrete jumps corresponding to one element in front of the crack tip. Several methods are reported in the literature and the fundamental difference is when to release the crack tip node in the loading cycle and when to estimate the crack opening/closure after the node release. Many researcher proposed the crack growth at maximum load and this was suggested by Newman [12]. Others released the node at minimum load and obtained similar results same as maximum load node release scheme. Alizadeh *et al.*[13] conducted a systematic analysis of the four most commonly used node release scheme and the results are discussed in Figure 1.12 and Figure 1.13.

Constraint Effect

The 2D plane strain state often used in finite element simulations as an idealization of the condition in the interior of a 3D fatigue crack. It is expected that the constrain effect will decrease in case of gross plastic deformation around the crack tip. McClung and Sehitoglu [14] mentioned that the state of stress which is plane strain in the interior of the crack and plane stress on the surface under LEFM conditions, will be plane stress throughout the specimen for gross plastic deformation.
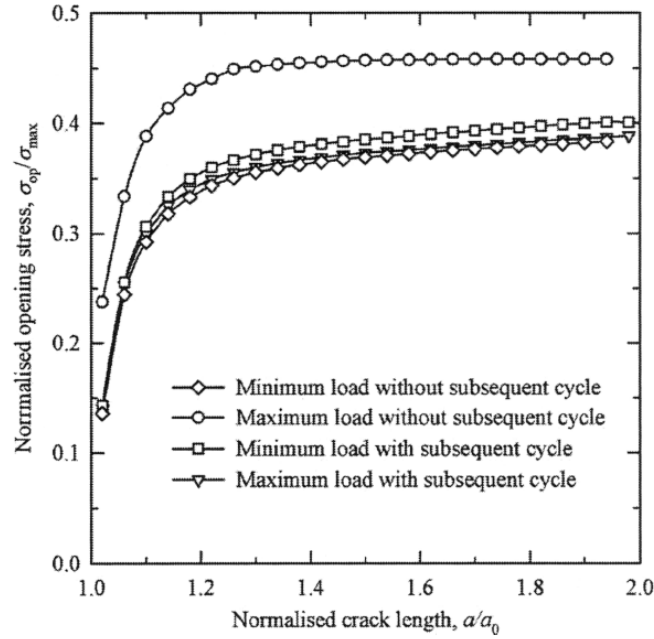
Figure 1.13: Crack closure result from different node release scheme [13]
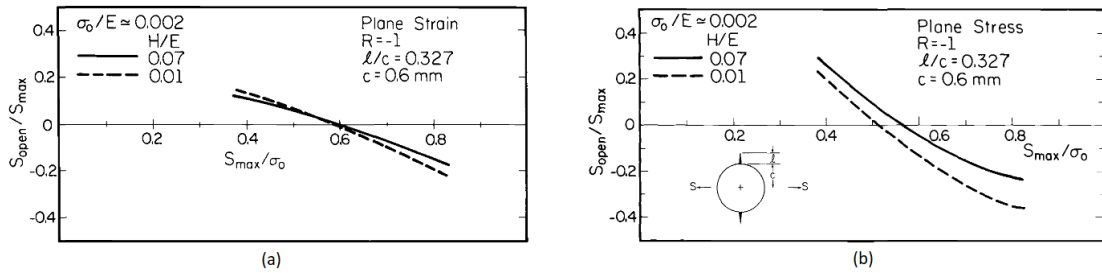
Figure 1.14: The crack opening levels obtained numerically for a crack growing out from a hole in two different materials. [15]

Numerical Results of Crack Closure Simulations

Lalor and Sehitoglu [15] studied the crack opening and closing level of a fatigue crack growing from a notch and the results are independent of the notch affected region. A 2D FE model is used to study in both plane stress and plane strain under load control. Two different constitutive models are used; both bilinear elastic-plastic kinematic hardening model with different ratios between the hardening modulus H and elastic modulus E. The crack opening results for plane stress and strain is shown in Figure 1.14

The difference between the crack opening and closure level is more significant in LCF regime. The closure level decreases more compared to the opening as the loading condition goes outside small scale yielding. McClung and Sehitoglu [14] use the crack opening level calculated using modified Dugdale model by Newman and compared it with experimental results as shown in Figure 1.14. To take strain hardening into account an average of the yield stress and ultimate tensile strength is used as yield limit in the model. The general behavior of Newman's crack opening
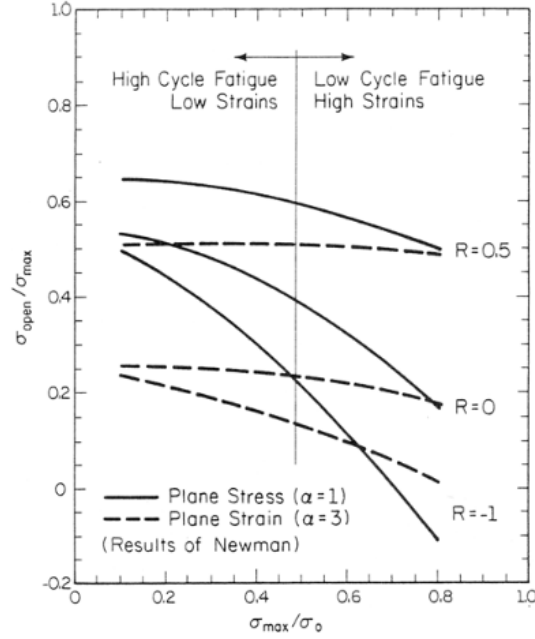
Figure 1.15: The crack opening levels obtained numerically for a crack growing out from a hole in two different materials. [14]

model is shown in Figure 1.15.

In paper 37, the authors performed FEA simulation in ABAQUS. The material model used in the analysis is cyclic plasticity model with power-law hardening and masing behavior. An axi-symmetric model with an internal crack is meshed at element to crack length ratio in front of crack tip of $\frac{1}{2000}$ (refined mesh) and $\frac{1}{200}$ (coarse mesh). Node release scheme is used to release nodes such that the crack growth increment corresponds approximately to the crack-tip opening. A trial and error method is used to choose crack growth increment per cycle to be same order as $\Delta CTOD$. Simulation was continued until normalized crack-tip opening displacement ($\Delta CTOD/a$) reach a constant plateau. Opening level is calculated as the stress in the element in front of the crack-tip becomes tensile for the first time.

In thesis we use the method performed by S.Pommier et. al [38] in ABAQUS. Chaboche Plasticity Model is used with Von mises yield criterion. All the computations are performed under plane strain condition. Node release scheme is used to release the nodes at maximum strain amplitude. Two cycles per crack length is simulated and the crack opening level is determined at the second cycle for each crack length. The crack is considered to be opened when the displacement of the second node behind the crack-tip has reached 1.5% of its maximum value for a given crack length as shown in Figure 1.16.

Now researchers [39] are trying to incorporated XFEM in combination with visco-plastic constitutive model which is the high temperature Plasticity model with Z and n as visco-plastic parameter along with Chaboche material parameters. The simulations are performed in ABAQUS with Strain accumulation criteria for crack growth. The crack grows when accumulated plastic strain reached a particular value at the crack tip. Crack growth direction is orthogonal to that of the maximum
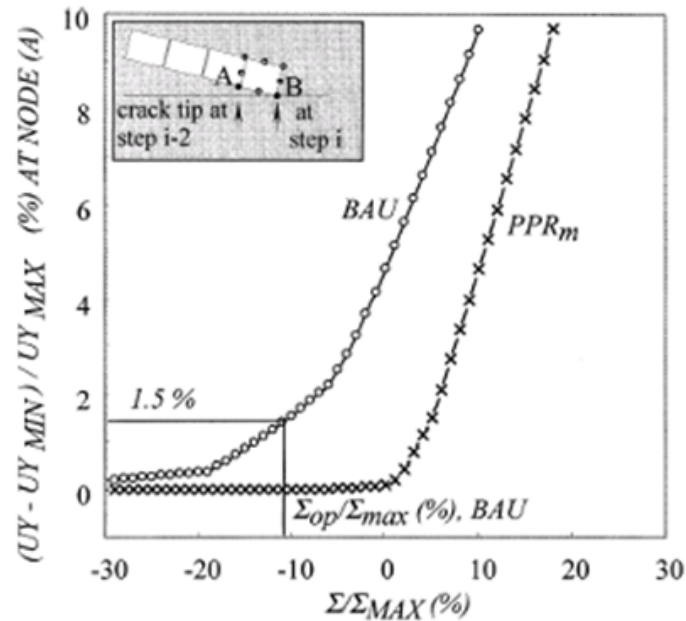
Figure 1.16: Crack closure level determination from COD vs Stress graph [38]
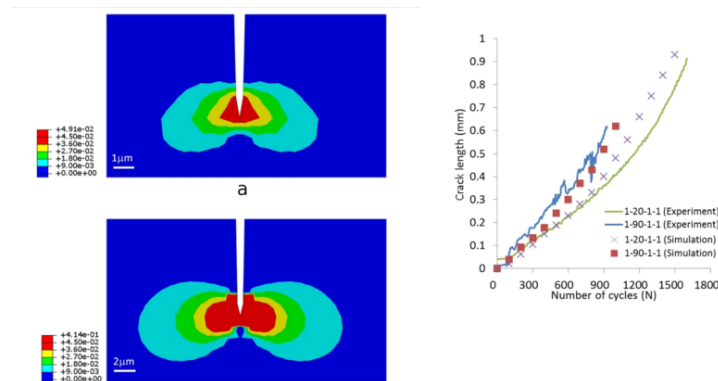
Figure 1.17: Crack length vs Time experimental vs simulation[39]

principal strain. The predicted crack growth rate using XFEM is in comparison with the experimental crack growth as shown in Figure 1.17.

Outline

The thesis is structured as follows:

The first Chapter it is done the study of crack propagation in low cycle fatigue. The main focus is on how different authors used to measure crack opening level in the past. It was seen that most of them used compliance based techniques. Then digital image correlation is introduced and its application in fatigue crack propagation is discussed. Then the finite element simulations done by different researchers in the past is discussed. The main technique is node release scheme whose four categories are detailed.

The second chapter presents the overview of Chaboche plasticity model. Followed by the low cycle fatigue experiment without pre-crack. The results of the experimentation is analyzed and the material parameters for Chaboche model is determined. This parameters are used to simulate the material model in ABAQUS and the results are compared with experiments.

The third chapter presents the finite element simulation of plasticity induced crack closure in Low Cycle Fatigue. The results of the finite element simulation is used to determine the reference crack opening level using method of Pommier as shown in Figure 1.16. Then the Crack Opening Displacement (COD) versus Stress curve is post processed for different lengths of extensometer and different distance from the crack tip. From the COD versus Stress hysteresis curve a method is developed to calculate the opening level whose value is same as that of reference opening level. Then, the effect of noise on the COD vs Stress hysteresis loop is simulated in order to be comparable to actual experiment,since DIC experiments contains noise of some level.

The fourth chapter presents the experimental campaign conducted on the KSA30 material. The experimental setup for DIC measurement of crack propagation has been discussed. The method developed in previous chapter is applied and crack opening level is determined. The FEM opening level is compared with the experimental values.

Chapter 2

Material Model Parameters Identification

The main aim of this thesis is to simulate plasticity induced crack closure in Low Cycle Fatigue. In order to do that it was selected two materials, A4T (25CrMo) and KSA30 (30NiCrMoV12) are special steels with high mechanical properties and thermally treated. These are high strength steels used for the manufacturing of railway axle and turbine shaft. The main properties of these materials are that they show cyclically softening behavior during constant strain amplitude loading.

In order to simulate, the material properties in Finite Element Software ABAQUS, it is required to select a material model for the particular application. In this case, it is known that the material will undergo cyclic plasticity during the loading, a suitable cyclic plasticity model is required to be chosen. After consulting previous literatures it was arrived that Chaboche plasticity model (in ABAQUS) is powerful enough to model and implement combined hardening, cyclic hardening, softening and ratcheting in FEM.

2.1 Chaboche Material Model

Before calculating the material model parameters a brief overview of Chaboche model is provided. For cyclic plasticity models there are three elements which defines the model. They are as follows:

2.1.1 Yield Function

Yield function describes a combination of stresses needed to initialize plastic deformation. Generally, Von Mises and Tresca criteria is used in modeling (Refer Figure 2.1a). Chaboche model uses Von Mises failure criteria is used as yield function as shown in Figure 2.1b. The yield surface is defined by the function as shown in Equation 2.1.

$$f = (\underline{s} - \underline{\alpha}) : (\underline{s} - \underline{\alpha}) - 2k^2 \tag{2.1}$$

The terms in this equation are as follows:

(a) Von Mises Vs Tresca Criterion   (b) Von Mises Yield Surface
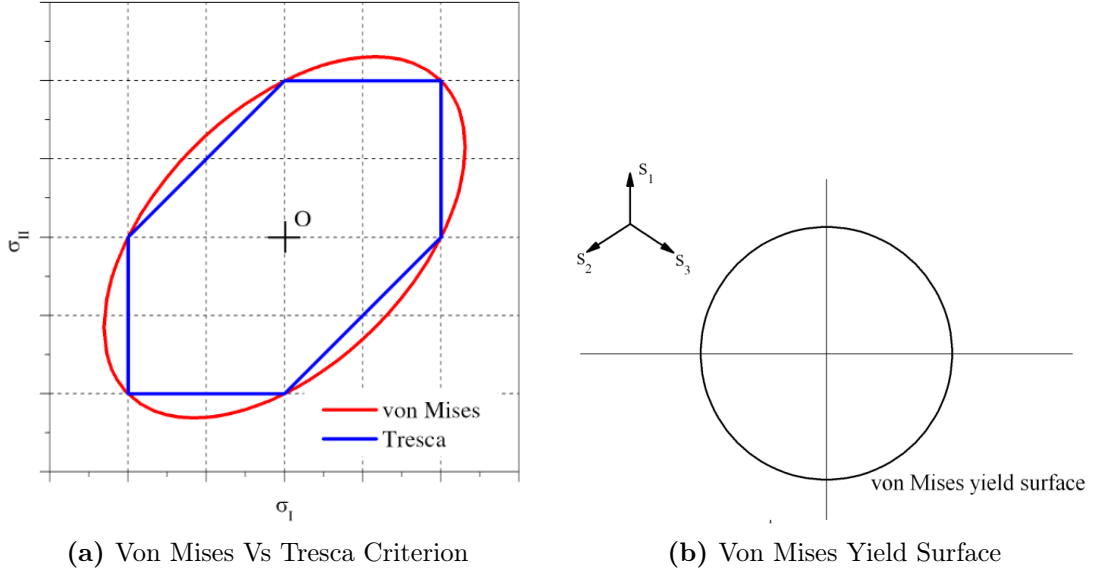
Figure 2.1: Yield Function

- $\underline{s}$ is the deviatoric stress vector;

- $\underline{\alpha}$ is the backstress vector;

- k is the shear yield stress;

- σ_0 is the yield stress in tension;

2.1.2 Flow Rule

Flow rule is the constitutive equation that defines the relationship between stresses and plastic strain increments. These equations are based on the normality postulate by Drucker, which states that the plastic strain increment vector is normal to the yield surface during plastic deformation:

$$d\underline{\varepsilon}^p = \sqrt{\frac{3}{2}}dp\underline{n} = \frac{1}{h}(d\underline{s}:\underline{n})\underline{n} \qquad (2.2)$$

The terms in this equation are as follows:

- $d\underline{s}$ is the deviatoric stress increment vector;

- $\underline{\varepsilon}^p$ is the plastic strain increment vector defined as; $dp = \sqrt{\frac{2}{3}(d\underline{\varepsilon}^p : d\underline{\varepsilon}^p)}$

- dp is the equivalent plastic strain increment;

- $\underline{n}$ is the exterior unit normal vector to the yield surface at the loading point defined as; $\underline{n} = \frac{\underline{s}-\underline{\alpha}}{\sqrt{2k}}$

- h is the plastic modulus function;

(a) Isotropic Hardening **(b)** KinematicHardening
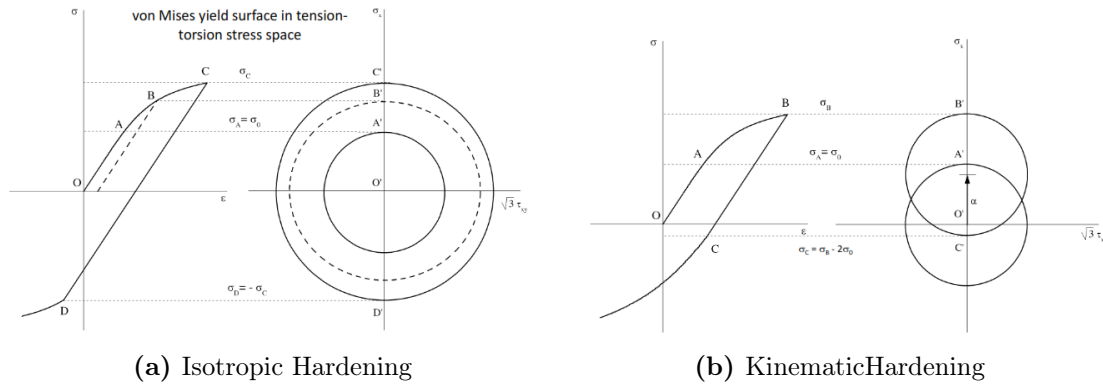
Figure 2.2: Hardening Rule

2.1.3 Hardening Rule

This rule describes how the yield surface is altered due to the plastic strain in order to satisfy the consistency condition. Consistency condition states that during elastic-plastic deformation the stress state remains on the yield surface.

This model includes two types of hardening rule:

- Isotropic hardening in which the yield surface expands with plastic strain. From Figure 2.2a, it can be seen that the yield surface evenly expands;

- Kinematic hardening in which the yield surface translates with plastic strain. From Figure 2.2b,it can be seen that the yield surface translates, without change in size;

2.1.4 Combined Hardening

Isotropic hardening and kinematic hardening is combined in Chaboche plasticity model to describe the transient effects such as strain hardening and softening, ratcheting and stress relaxation.

The hardening rule can be written in general form as:

$$f = (\underline{s} - \underline{\alpha}) : (\underline{s} - \underline{\alpha}) - 2k^2(p) = 0 \tag{2.3}$$

For pure kinematic hardening k is a constant, which imples the radius of the yield surface is constant as shown in Figure 2.2b. For pure isotropic hardening $\underline{\alpha} = \underline{0}$, which means the center of the yield surface remains constant, but radius increases after each cycle as shown in Figure **??**. Most of the materials A4T and KSA30 will show both kinematic and isotropic hardening until they become cyclically stable after which kinematic hardening rule is followed.

Mathematically, consistency condition is given by $df = 0$, from which we obtain the plastic modulus as a function of k and $\underline{\alpha}$:
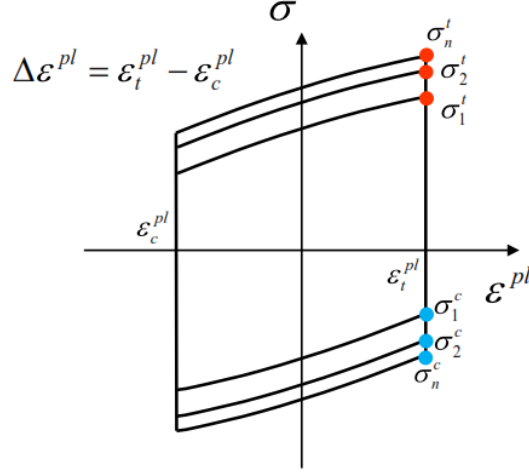
Figure 2.3: Isotropic Hardening parameter calculation

$$h = \sqrt{\frac{2}{3}\frac{n : d\underline{\alpha}}{dp}} + \frac{2}{\sqrt{3}}\frac{dk}{dp} \tag{2.4}$$

Isotropic hardening can be described by specifying the equivalent stress defining the size of yield surface k as the function of equivalent plastic strain. The following relationship holds:

$$k(p) = \frac{\sigma_0(p)}{\sqrt{3}} \tag{2.5}$$

where $\sigma_0(p)$ can be defined by using Voce equation as follows:

$$\sigma_0(p) = \sigma|_0 + Q_\infty(1 - e^{-bp}) \tag{2.6}$$

The constant term of this equation, $\sigma|_0$ is the yield stress of the first loading cycle and p is the equivalent plastic strain. The term Q_{inf} and b are constants of the material and they are extracted from the results of symmetric strain controlled cyclic experiments. As shown in Figure 2.3, the experimental hysteresis curves are plotted on a (ε^p, σ) graph. Considering each ith cycle, the value of $\sigma_{0,i}$ is estimated as:

$$\sigma_{0,i} = \frac{\sigma_i^t - \sigma_i^c}{2} \tag{2.7}$$

The equivalent plastic strain increment, p, is defined for each cycle as:

$$p = \varepsilon_x^p = (\frac{1}{2}(4i - 3)\Delta\varepsilon^p) \tag{2.8}$$

Therefore, all the collected $\sigma_{0,i}$ and p_i values are fitted to obtain Q_∞ and b.

The kinematic hardening component is defined as the combination of a purely kinematic term (linear Zeigler hardening law) and a relaxation term, which introduces non-linearity [??]
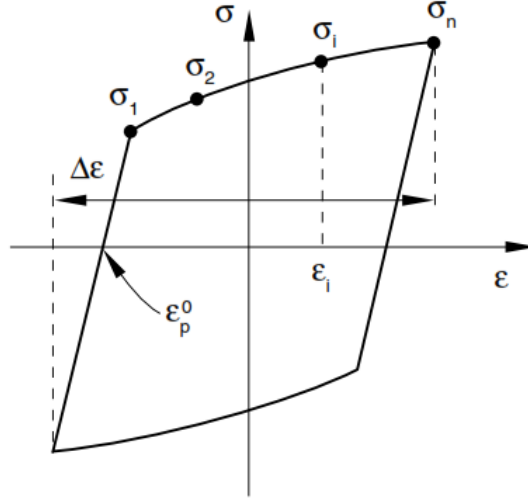
Figure 2.4: Kinematic Hardening parameter calculation

$$d\underline{\alpha} = \frac{2}{3}Cd\underline{\varepsilon}^p - \gamma\underline{\alpha}dp \qquad (2.9)$$

Integrating the back-stress evolution law, we obtain:

$$\sigma - \sigma_0 = \frac{C}{\gamma}(1 - e^{-\gamma(\varepsilon_p - \varepsilon_p^1)}) + (\sigma_1 - \sigma_0)e^{-\gamma(\varepsilon_p - \varepsilon_p^1)} \qquad (2.10)$$

This equation is utilized to fit the stabilized upper half cycle of an unidirectional symmetric strain-controlled test, as shown in Figure 2.4.

σ_0 is given by the relationship:

$$\sigma_0 = \frac{\sigma_1 - \sigma_{min}}{2} \qquad (2.11)$$

Chaboche model allows for the superposition of several kinematic hardening components (backstresses), which helps in considerably improving the result. Normally, it is optimum to use 3 backstresses even though ABAQUS allows for maximum 5.

Each single kinematic term can be written as:

$$d\underline{\alpha}^k = \frac{2}{3}C_k d\underline{\varepsilon}^p - \gamma_k\underline{\alpha}^k dp \qquad (2.12)$$

The overall backstress is the sum of all the backstresses:

$$\underline{\alpha} = \sum_{i=1}^{N} \underline{\alpha}^{(k)} \qquad (2.13)$$

The fitting procedure with one backstress only can be applied to each single backstress, considering the following equation for k^{th} backstress:

$$\sigma^k - \sigma_0^k = \frac{C_k}{\gamma_k}(1 - e^{-\gamma_k(\varepsilon_p^k - \varepsilon_{p,1}^k)}) + (\sigma_1^k - \sigma_0^k)e^{-\gamma_k(\varepsilon_p^k - \varepsilon_{p,1}^k)} \qquad (2.14)$$

A4T Specimen No.	Strain Amplitude (%)	KSA30 Specimen No.	Strain Amplitude (%)
1	0.6%	1	0.35%
2	0.6%	2	0.35%
3	1.0%	3	0.5%
4	1.0%	4	0.5%
5	1.5%	5	0.8%
6	1.5%	6	0.8%

Table 2.1: Strain Amplitude applied on materials
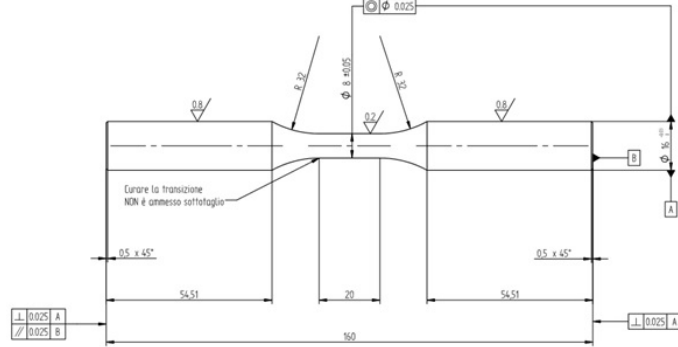
Figure 2.5: Specimen for Strain-Controlled LCF Testing

In the next section, it is discussed about the procedure to conduct the symmetric low cycle fatigue experiment and determination of isotropic hardening and kinematic hardening parameters.

2.2   Low Cycle Fatigue Experiment without percrack

Before analyzing and obtaining the parameters for Chaboche material model, an experimental investigation is required to be conducted on A4T and KSA30. The result from the experimental investigation is analyzed as per the theory mentioned in the previous section to give three isotropic hardening and six kinematic hardening parameters. For this thesis, author used the data of already conducted Low Cycle Fatigue experimental data in the identification of Chaboche Model parameters. Nevertheless the details of this LCF experiment are explained in this section.

The LCF tests were performed at ambient temperature imposing 3 different strain ranges for A4T and KSA30 ($\Delta\varepsilon_1, \Delta\varepsilon_2, \Delta\varepsilon_3$) as shown in Table 2.1. Cylindrical specimen without pre-crack as shown in Figure 2.5. All the tests were performed consistently with the reference standard ASTM E 60692 Standard Practice for Strain-Controlled Fatigue Testing [40]. All these tests were run controlling the applied strain as shown in Figure 2.6 and imposing a strain ratio R_ε equal to -1.

All the LCF tests were conducted on a MTS-810 servo-hydraulic testing machine capable of applying a load up to 100 kN available at Politecnico di Milano, Depart-
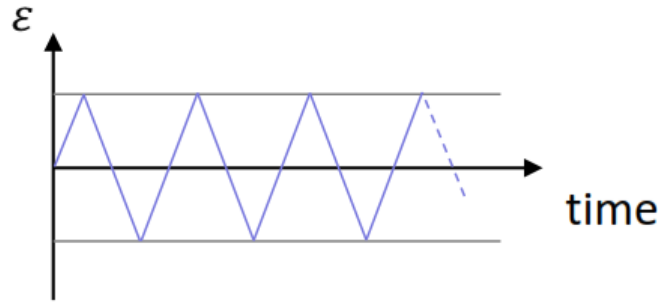
Figure 2.6: Specimen for Strain-Controlled LCF Testing
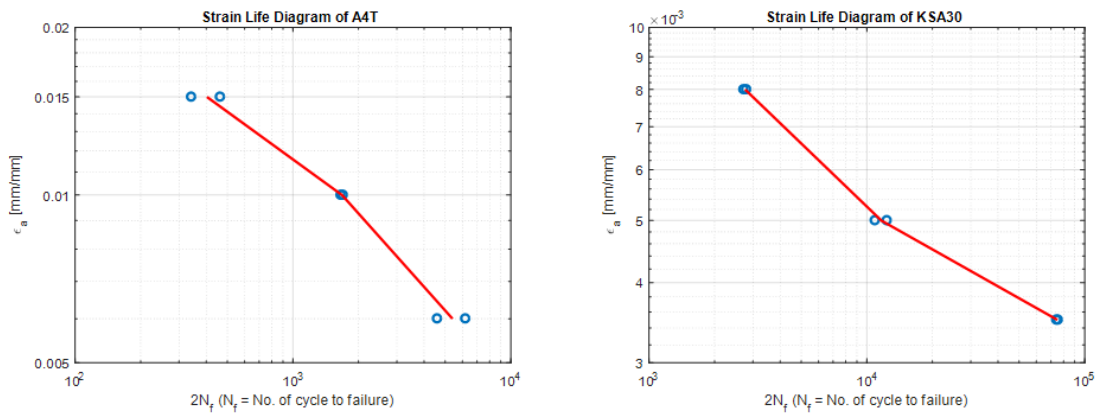
Figure 2.7: Strain Life diagram of A4T (Left) and KSA30 (Right)

ment of Mechanical Engineering. The testing machine alignment was performed as per standard ISO-12106 (*Metallic Materials - Fatigue Testing- Axial-Strain-Controlled Method*) and ASTM E1012 (*Standard Practice for Verification of Test Frame and Specimen Alignment Under Tensile and Compressive Axial Force Application*). All the measurements showed that the bending component is always lower than 5%, as required by the standards.

The strain life diagram from the experiment for A4T and KSA30 is shown in the Figure 2.7. The difference in the curve is mainly due to the strain amplitudes at which the experiments were performed. It can be seen that the LCF experiment for A4T were performed at higher strain amplitudes than KSA30 material.

2.2.1   Analysis of the experimental results

The results obtained from the experiments are analyzed to build a complete Chaboche model that can be used for FEM simulations.

Figure 2.8: Experimental Hysteresis Loop of A4T (Left) and KSA30 (Right)

Strain Amplitude	$Q_\infty[MPa]$	b	$k[MPa]$
0.6%	-43.8	1.03	239.3
0.6%	-48.6	1.18	245.7
1.0%	-40.7	0.52	230.7
1.0%	-33.6	0.43	222.3
1.5%	-69.0	2.79	263.7
1.5%	-22.3	1.26	216.5
Average	-43.0	1.20	236.4

Table 2.2: Isotropic Hardening Parameters of A4T Steel

2.3   Parameter Identification of A4T

Isotropic Hardening Parameters of A4T

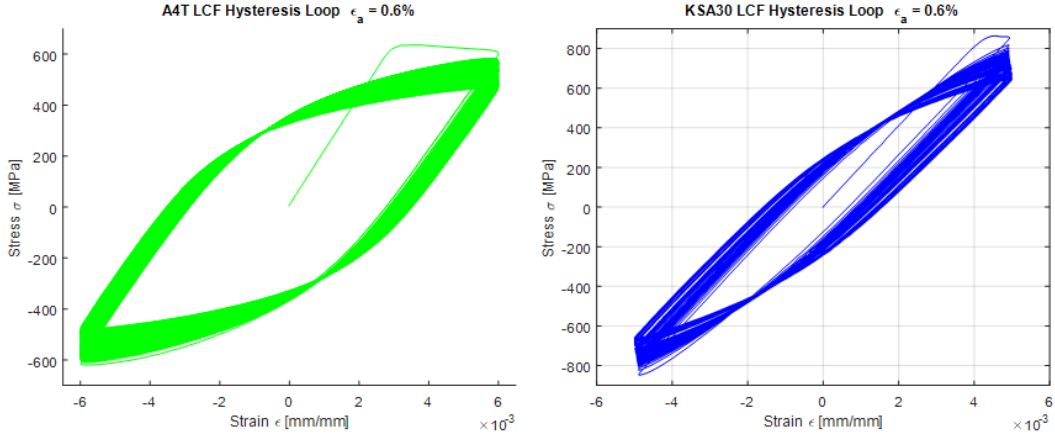Isotropic hardening parameters are obtained by fitting the curve between cumulated plastic strain (ε_{pl}) in X-axis and yield stress (σ_0)in Y-axis. The Voce model as shown in Equation 2.6 is adopted to fit the curve. From Figure 2.9 for 0.6% strain amplitude, Figure 2.10 for 1.0% strain amplitude, Figure 2.11 for 1.5% strain amplitude, we can see that this equation cannot model a quick drop in yield strength. The mean value of six isotropic hardening parameters from three different strain amplitudes are taken and tabulated as shown in Table 2.2.

Kinematic Hardening Parameters of A4T

Kinematic hardening parameters are obtained by using the hysteresis curve which taken at half of the failure life ($\frac{N_f}{2}$). Only upward branch of the stabilized hysteresis loop is considered as shown in Figure 2.12 (Left). Then the elastic part of the total deformation is removed from the upward branch of the stabilized hysteresis loop as shown in Figure 2.12 (Right). Finally, σ_1 and ε_1 are defined using the σ_{end}^0 of the asymptotic isotropic curve. The non-linear kinematic hardening law with three backstress terms are fitted as shown in Figure 2.13. The fitting is performed using least square fitting function in MATLAB. From this fitting, we
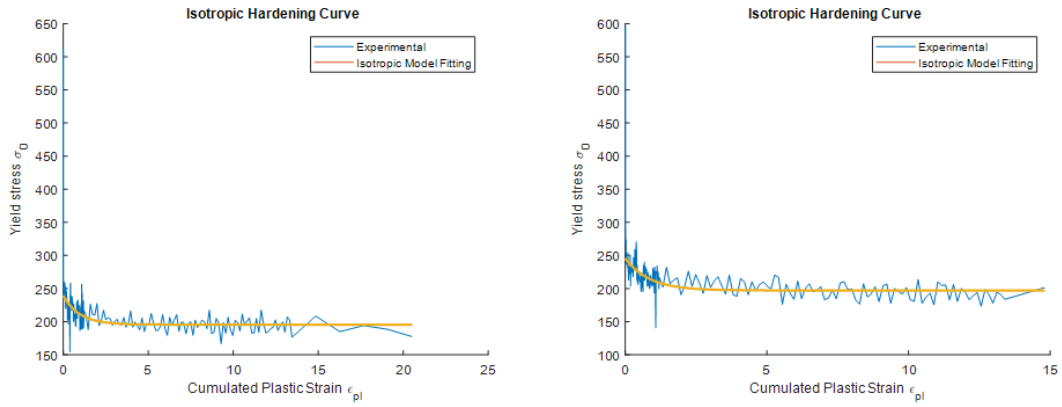
Figure 2.9: Istropic Hardening Model Fitting at $\varepsilon_a = 0.6\%$
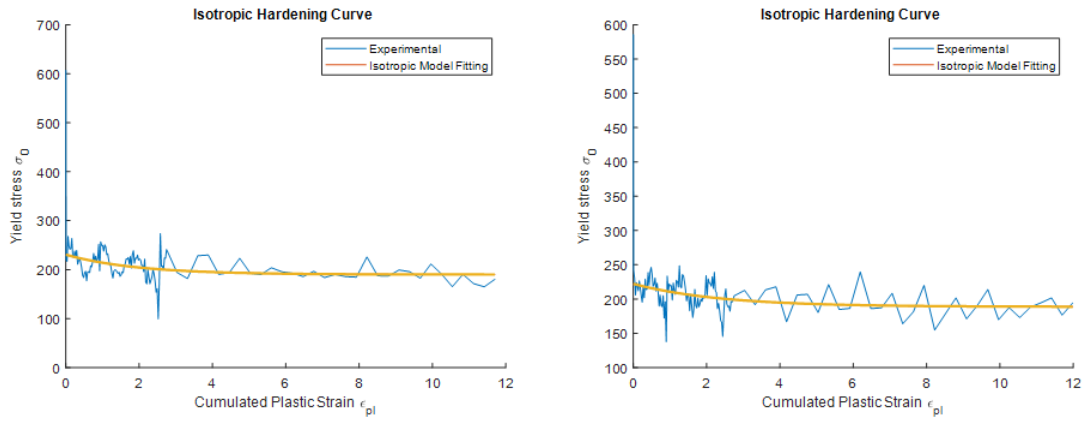
Figure 2.10: Istropic Hardening Model Fitting at $\varepsilon_a = 0.6\%$
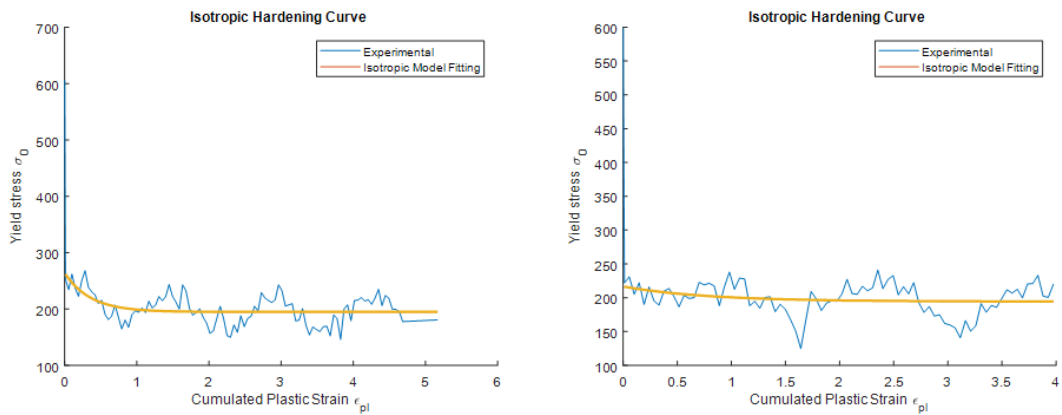
Figure 2.11: Istropic Hardening Model Fitting at $\varepsilon_a = 0.6\%$
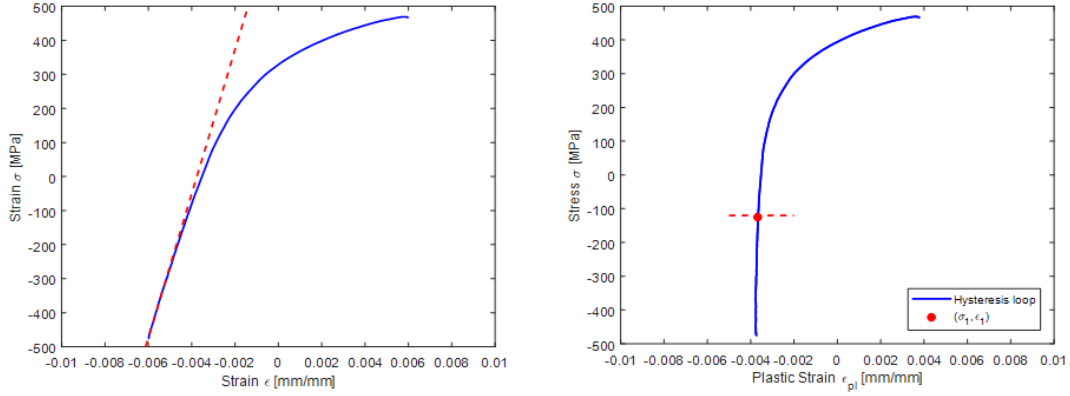
Figure 2.12: Upper Part of Hysteresis Loop (Left) and Stress Vs Plastic Strain (Right)
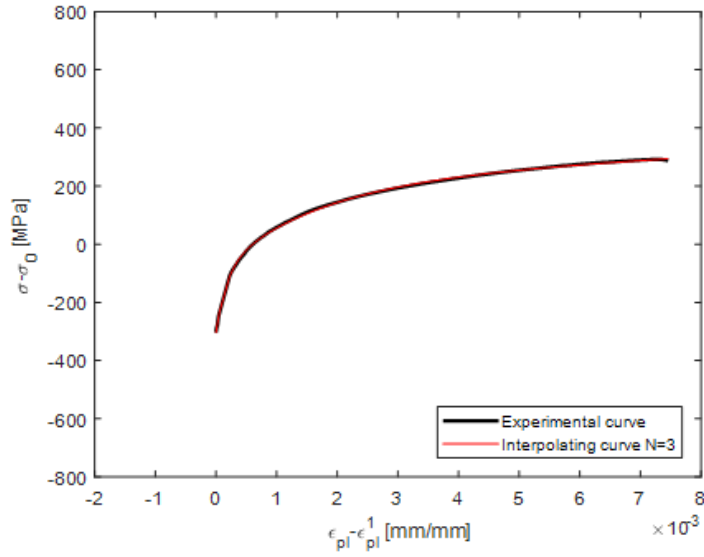
Figure 2.13: Three backstress fitting for $\varepsilon_a = 0.6\%$

obtain $C_1, \gamma_1, C_2, \gamma_2, C_3, \gamma_3$ for each strain amplitude. The value of γ_3 should be near to zero. So in the fitting it is fixed as 0.01. The reason for this approach is high value of γ_3 can over predict rathcetting. The kinematic fitting for 1.0% strain amplitude and 1.5% strain amplitude are shown in Figure 2.14 and Figure 2.15 respectively. The kinematic hardening parameters are tabulated as shown in Table 2.3.

2.3.1   Combined Hardening Simulation - A4T

Once the Chaboche model parameters are identified, the finite element simulation is performed in ABAQUS to compare the material model results with experimental. For this, a cube of 1 mm x 1 mm x 1 mm is meshed in ABAQUS with a single element and boundary conditions as shown in Figure 2.16. The sinusoid load is applied with amplitude equal to required strain amplitude. For example, if one
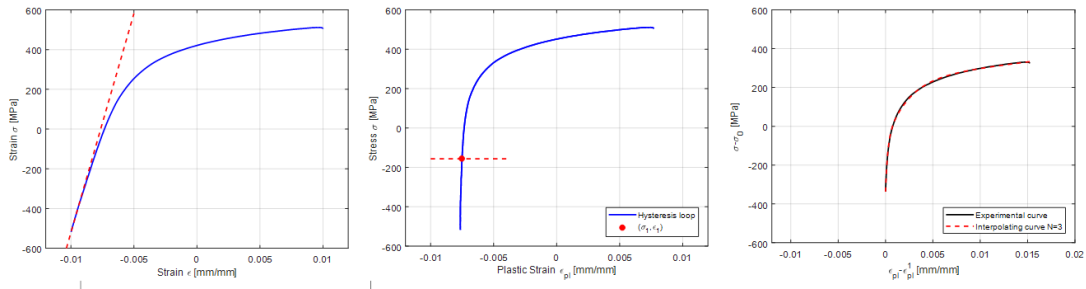
Figure 2.14: Three backstress fitting for $\varepsilon_a = 1.0\%$
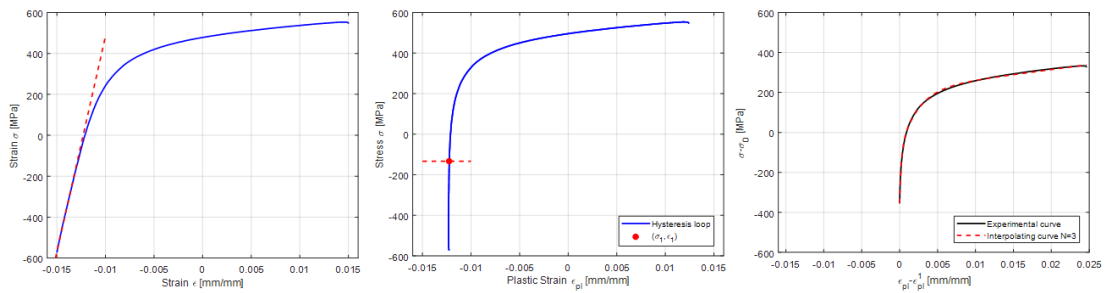
Figure 2.15: Three backstress fitting for $\varepsilon_a = 1.5\%$

Strain Amplitude	C_1	γ_1	C_2	γ_2	C_3	γ_3
0.6%	642453	4500	99099	425	4263	0.01
0.6%	489920	4500	103826	425	4148	0.01
1.0%	638203	4500	84462	425	6442	0.01
1.0%	584813	4500	81013	425	5031	0.01
1.5%	636478	4500	81013	425	5031	0.01
1.5%	588813	4500	89994	425	4624	0.01
Average Value	596780	4500	91480	425	5083	0.01

Table 2.3: Kinematic Hardening Parameters of A4T Steel
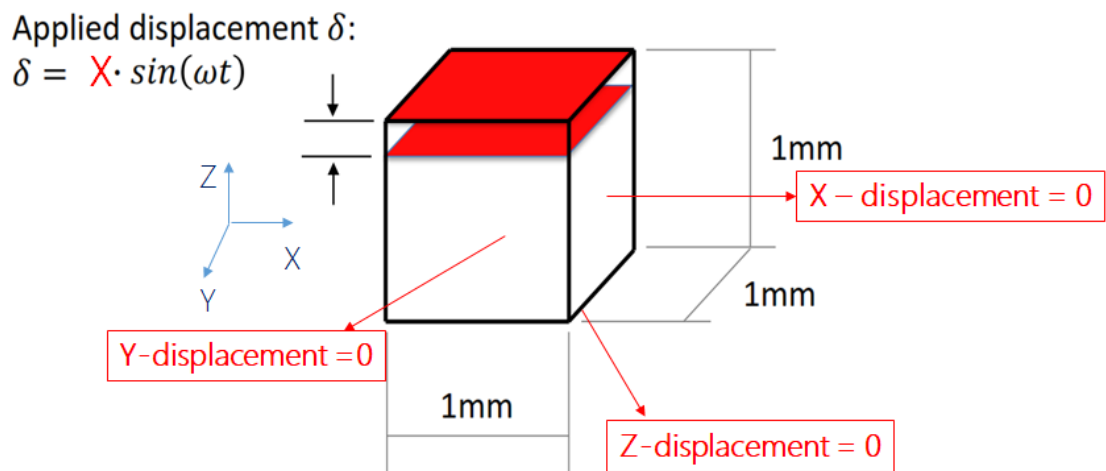
Figure 2.16: Model to simulate material behavior of A4T
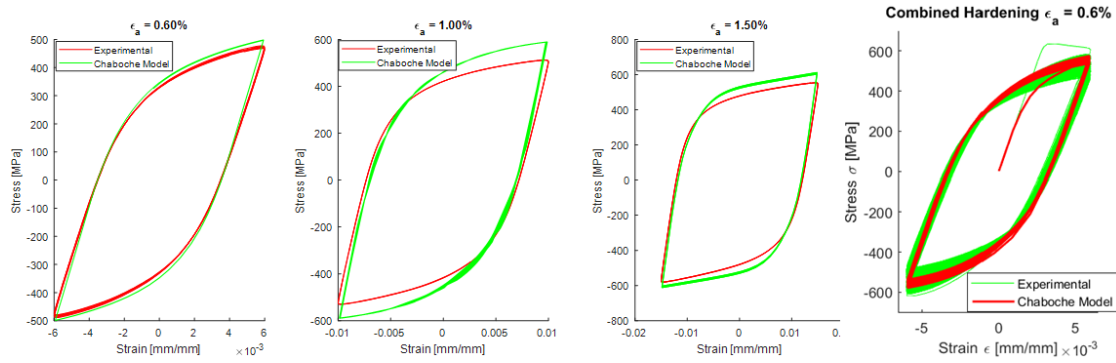
Figure 2.17: A4T Experimental Versus Chaboche Model
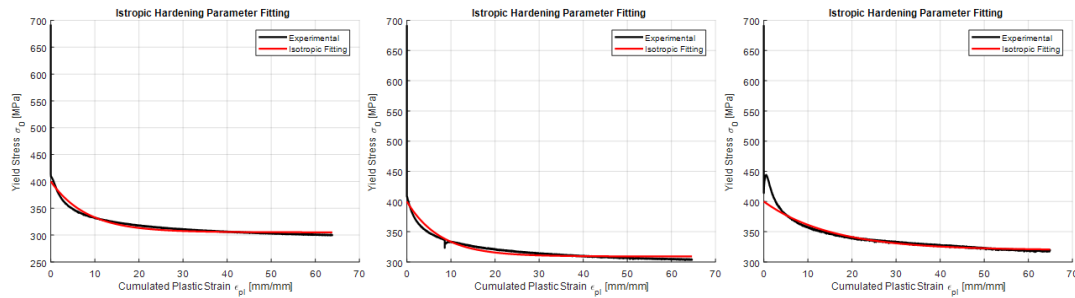
Figure 2.18: Isotropic Curve Fitting for $\varepsilon_a = 0.35\%$

want to simulate for 0.6% strain amplitude, the «X» in the figure 2.16 should be 0.006 mm. The results for A4T are shown in Figure 2.17. The experimental hysteresis loops are compared with simulated one at different strain amplitude and a combined hardening stress-strain plot for 0.5% strain amplitude.

2.4   Parameter Identification of KSA30

Isotropic Hardening Parameters of KSA30

Isotropic Hardening Parameters for KSA30 are calculated with the same method for A4T. The curve fitting is shown in Figure 2.18, Figure 2.19 and Figure 2.20. The results are tabulated in Table 2.4.
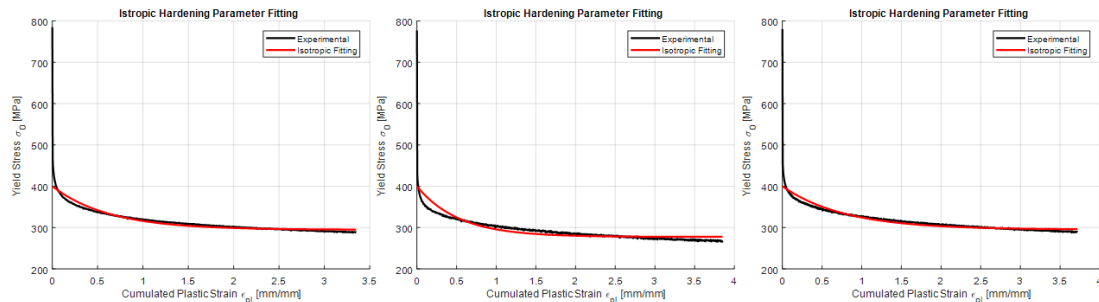
Figure 2.19: Isotropic Curve Fitting for $\varepsilon_a = 0.50\%$
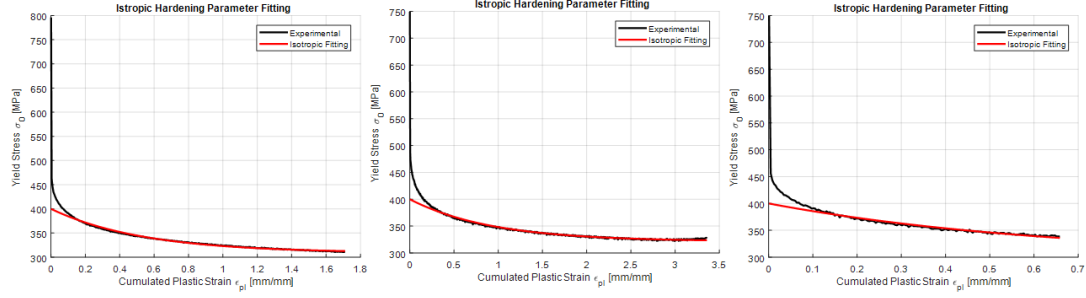
Figure 2.20: Isotropic Curve Fitting for $\varepsilon_a = 0.80\%$

Strain Amplitude	Q_∞	b	k
0.35%	-94.8	0.12	400
0.35%	-90.9	0.13	400
0.35%	-80.5	0.07	400
0.50%	-126.42	2.28	400
0.50%	-122.7	1.9	400
0.50%	-122.4	1.97	400
0.80%	-91.3	1.85	400
0.80%	-78.68	1.07	400
0.80%	-101.27	1.53	400
Average	-106.3	1.07	400

Table 2.4: Isotropic Hardening Parameters of KSA30 Steel

Kinematic Hardening Parameters of KSA30

Kinematic Hardening Parameters for KSA30 steel are calculated with the same method for A4T steel. The curve fitting is shown in Figure 2.21, Figure 2.22 and Figure 2.23. The results are tabulated in Table 2.5.

2.4.1   Combined Hardening Simulation- KSA30

The combined hardening simulation is performed in ABAQUS same as the procedure of A4T and the results are shown in Figure 2.24. The experimental hysteresis loops are compared with simulated one at different strain amplitude and
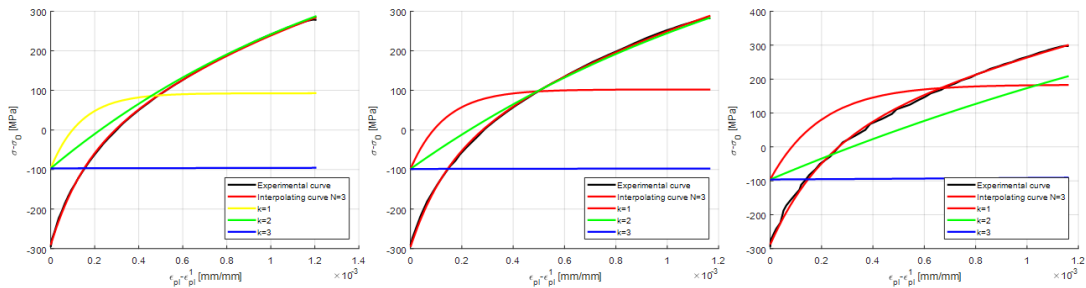
Figure 2.21: Backstress Curve Fitting for $\varepsilon_a = 0.35\%$

Strain Amplitude	C_1	γ_1	C_2	γ_2	C_3	γ_3
0.35%	842496	5000	275094.3	350	4500	0.01
0.35%	906367	5000	275772	350	4500	0.01
0.35%	917352	5000	285672	350	4500	0.01
0.50%	996760	5000	167472	350	4500	0.01
0.50%	953469	5000	148783	350	4500	0.01
0.50%	791798	5000	157522	350	4500	0.01
0.80%	469600	5000	120619	350	4500	0.01
0.80%	872092	5000	116598	350	4500	0.01
0.80%	1000000	5000	115398	350	4500	0.01
Average	861104	5000	184770	350	4500	0.01

Table 2.5: Kinematic Hardening Parameters of KSA30 Steel
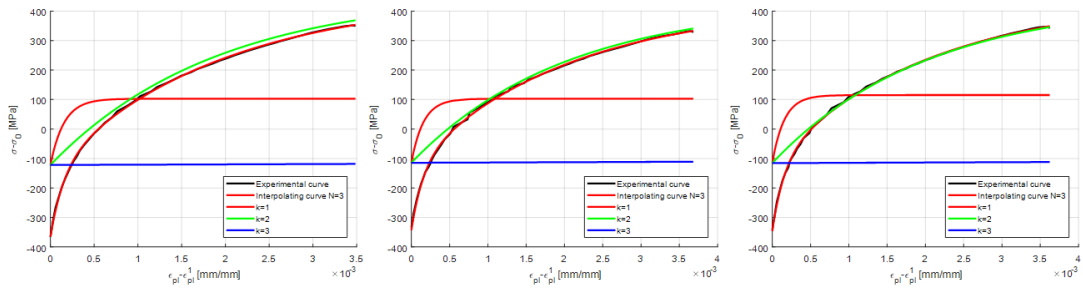
Figure 2.22: Backstress Curve Fitting for $\varepsilon_a = 0.50\%$
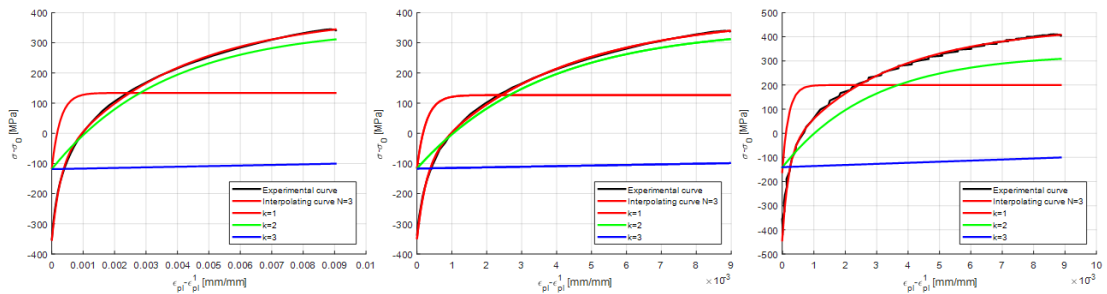
Figure 2.23: Backstress Curve Fitting for $\varepsilon_a = 0.80\%$
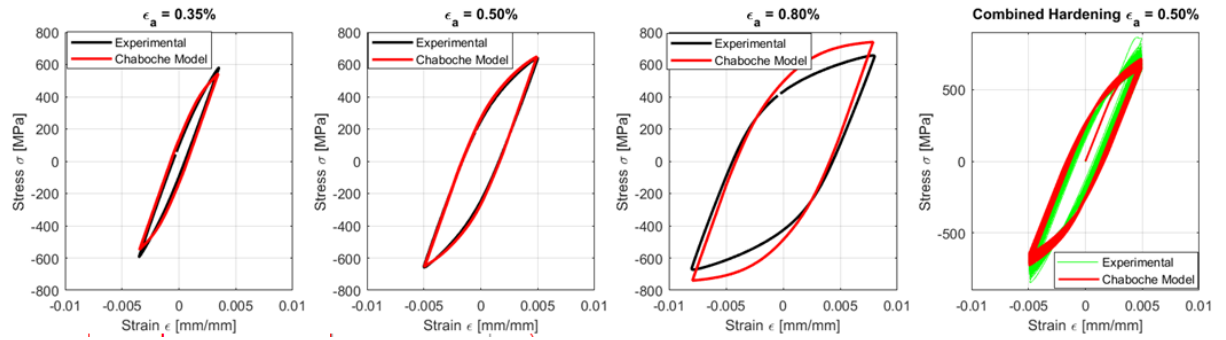
Figure 2.24: KSA30 Experimental Versus Chaboche Model

a combined hardening stress-strain plot for 0.5% strain amplitude.

From Figure 2.17 and Figure 2.24, it can be noted that one value of Chaboche model parameters cannot predict all the strain amplitudes with same accuracy. There can be variation depending on the value of strain amplitude. Also in the combined hardening simulation, due to the limitation of isotropic hardening model to describe the initial sudden drop in the yield stress, we can see that the the peak and valley stress amplitude of the simulated values in the initial cycles are lower than that of experimental values.

In the next section, crack propagation in Low Cycle Fatigue is simulated with the help of Chaboche cyclic plasticity model and results are discussed followed by comparison with the experimental data.

Chapter 3

Finite Element Simulation and Analysis of Crack Closure

3.1 Finite Element Simulation of Crack Closure

In this chapter, finite element simulation of a double edge-cracked plate tension specimen is performed. The constitutive behavior of the material is described by the Chaboche plasticity model whose parameters have been calculated in previous chapter. This model allows one to take in consideration kinematic and isotropic hardening for transient and stabilized cyclic plasticity and is provided in the ABAQUS code (version 6.14).

In property module section, material properties are assigned to the model. A4T and KSA30 is defined considering its;

- Elastic properties E and ν for Elastic Modulus and Poisson's ratio;

- Isotropic hardening coefficients k, C_∞ and b;

- Kinematic hardening coefficients $C_1, \gamma_1, C_2, \gamma_2, C_3, \gamma_3$;

The boundary conditions and the dimensions of the mesh that were used for the crack propagation computations are shown in Figure 3.1. Only half of the specimen is modeled using symmetric boundary condition on the crack line. The contact area and contact details are shown in Figure 3.2. All the computations have been conducted under the plane strain condition, using quadratic elements and a complete integration scheme. The crack growth is simulated using node release technique. The node is released after every 2 cycles, in order to stabilize the values of crack opening displacement in front of crack tip. Node is released at the peak of the strain amplitude cycle. A rigid contact surface is used in order to model only half of the specimen. Thus crack length is increased step-by-step after every two cycles. The mesh size along the crack axis is $20\mu m$. The crack is grown from $200\mu m$ to $500\mu m$ by releasing one element of $20\mu m$ every two cycles in order to stabilize the hysteresis loop at the crack tip. The determination of the crack opening level is performed at the second cycle for each crack length. As a matter of fact the hysteresis loop at the crack tip is stabilized at the second cycle. All the
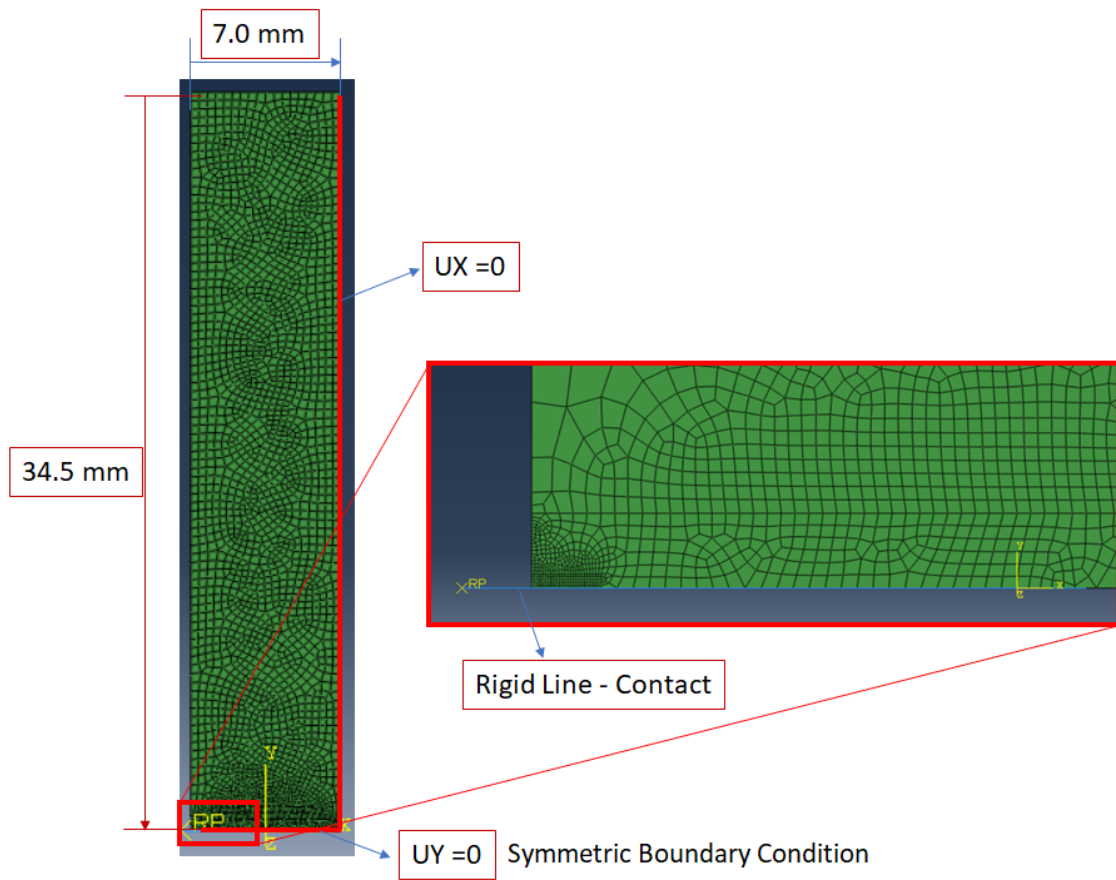
Figure 3.1: Model for Finite Element with Boundary Conditions
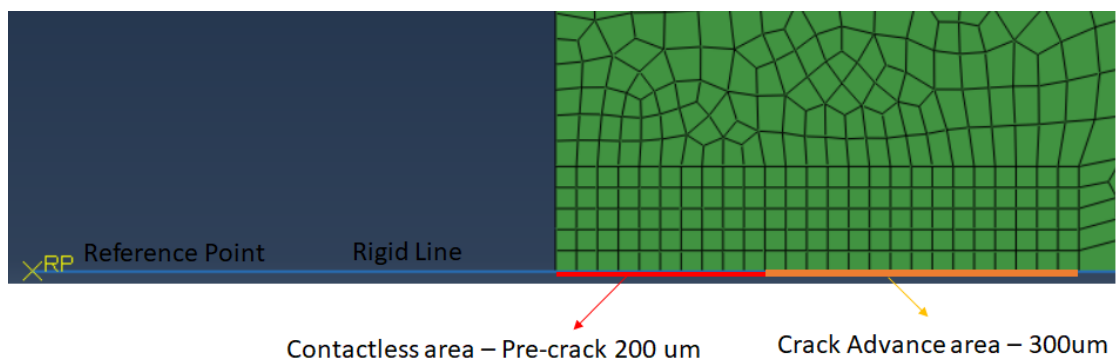
Figure 3.2: Model for Finite Element with Boundary Conditions
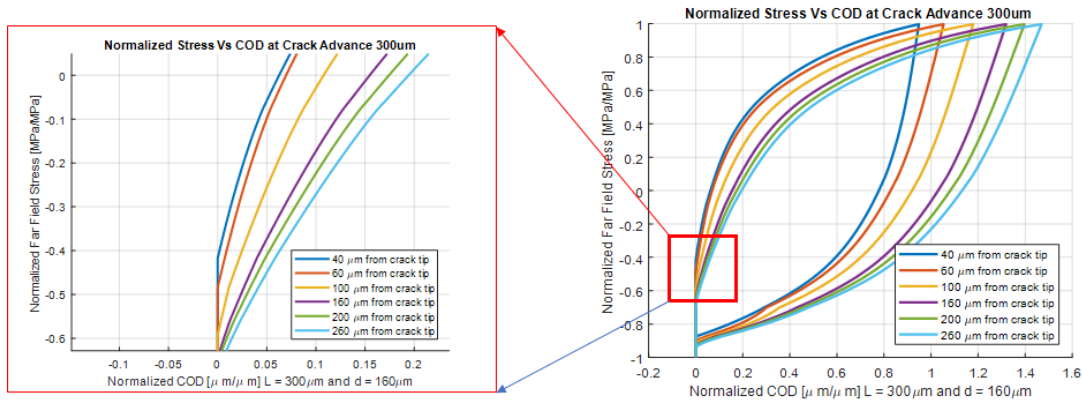
Figure 3.3: COD Vs Stress at crack flank for different distance from the crack tip
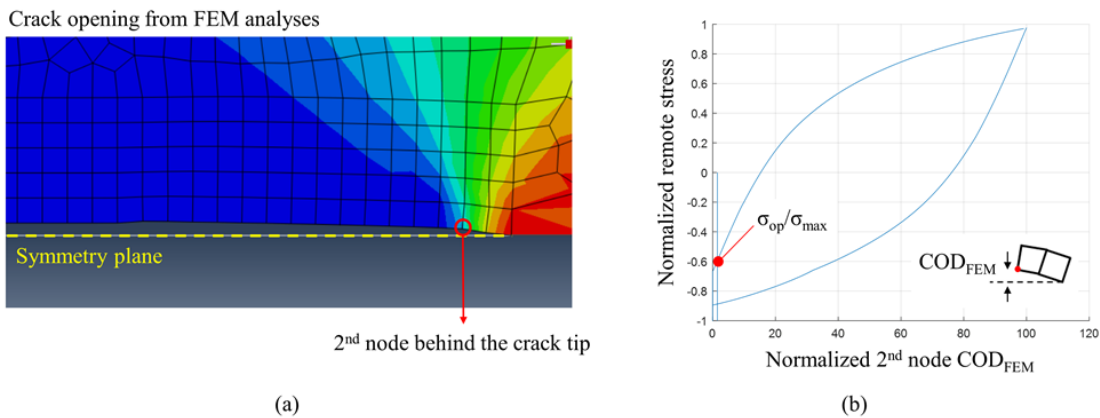
Figure 3.4: COD of Second Node from Crack Tip

computation are written as an ABAQUS input file through the software automated procedure.

It is seen that along the crack flank, the opening level decreases with increase in distance behind the crack tip as seen in Figure 3.3. So it is required a standard for an opening level determination against which we can compare the further analysis.

The opening level is determined for each step by using the method described by [38]. This paper states that *The ratio of the variation of the displacement of the displacement of the second node behind the crack tip (CTOD) with the maximum displacement of the node is plotted against the applied stress. When this ratio reaches 1.5%, the crack is assumed to be opened.* This is illustrated in Figure This criteria is used for all the simulations as reference crack opening level.

3.2   Plane Strain Results for A4T steel

The opening level and closing level behavior were analyzed for crack advance from $40\mu m$ to $300\mu m$ in Plane Strain condition at $\varepsilon_a = 0.4\%$. The results are plotted in Figure 3.5 . It can be noted that the crack opening and closing level happens at approximately same strain. This is same as the findings of Vormwald and Seeger [20].Initially the level is lower and it increases to a certain value then
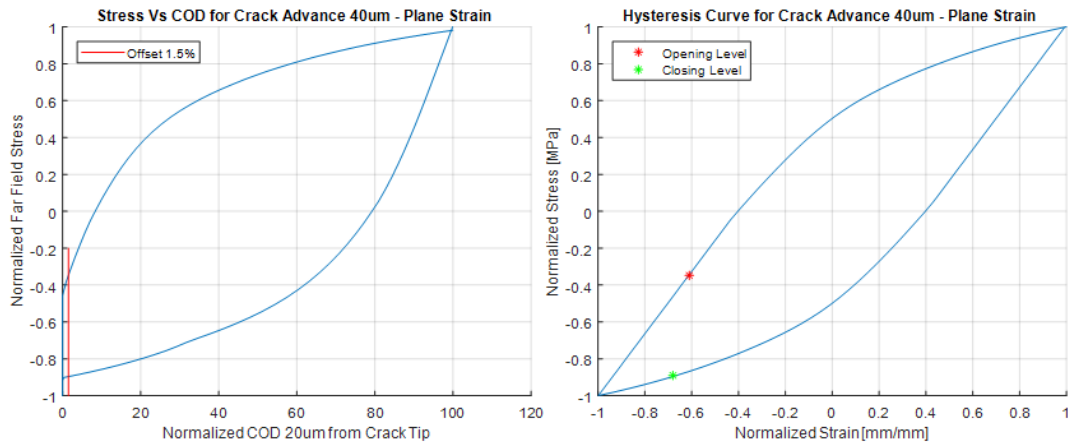
Figure 3.5: Opening and Closing Level for crack advance $40\mu m$ in Plane Strain
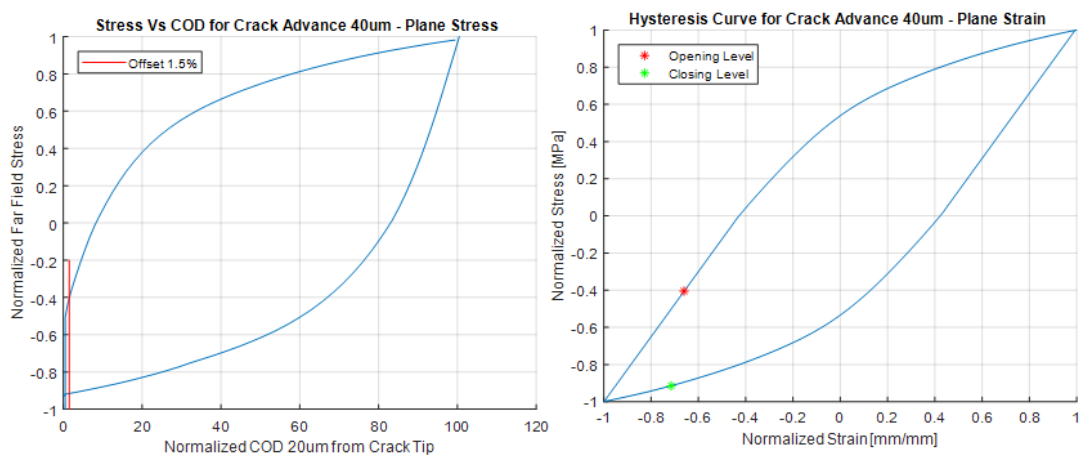
Figure 3.6: Opening and Closing Level for crack advance $40\mu m$ in Plane Stress

decreases as the crack advances. It can be observed that after a crack advance of $160\mu m$, the normalized opening level becomes constant. This is the expected behavior of crack opening level as the crack advances. From, this one can infer that the simulation is giving acceptable results.

3.3 Plane Stress Results for A4T steel

The opening level and closing level behavior were analyzed for crack advance from $40\mu m$ to $300\mu m$ in Plane Stress condition $\varepsilon_a = 0.4\%$. The results are plotted in Figure 3.6. The opening level behaves the same way as that of plane strain during crack advancement. From Figure 3.7, it can be observed that the normalized crack opening level in plane stress is 0.4 [MPa/MPa] lower than that of plane strain.

With this analysis, the author is confident that the simulation results are as expected and he can proceed further with development of method for estimation of opening level for digital image correlation experimental results.

Now the simulation opening level are measured with this method for both KSA30 and A4T for different strain amplitudes and the results are summarized in
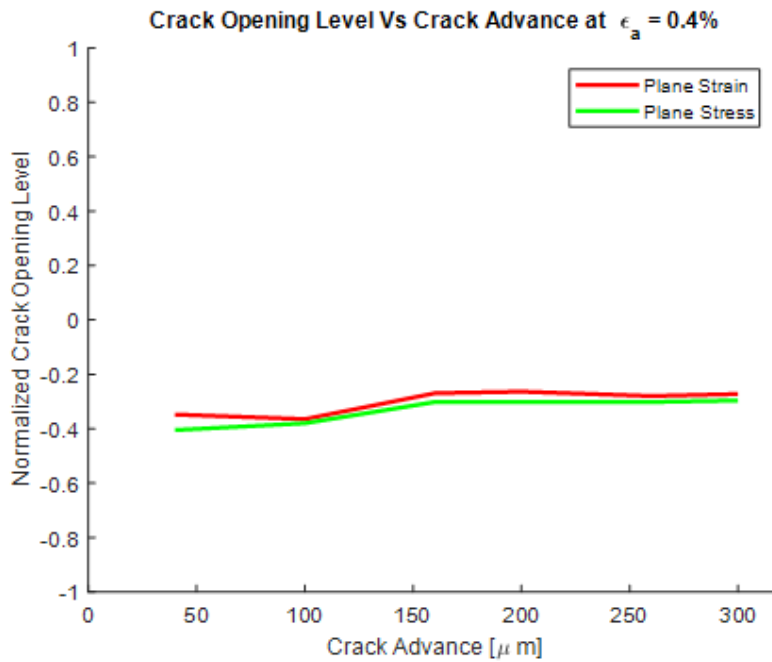
Figure 3.7: Opening Level as a function of crack advance for Plane Strain and Plane Stress

Figure 3.8.

3.4 Development of Method for Estimation of Opening Level for DIC

The main aim of this section is to develop a method, which we can use on the virtual extensometer data of DIC, which can provide reference opening level. In DIC, finding the exact crack tip location is a difficult task. One should be able to measure the opening level with much accuracy at a distance of $100\mu m$ and above from the crack tip. Also, it is needed to identify the length of extensometer to be used. The analysis steps are illustrated below:

3.4.1 Step 1: Reference Opening Level

First step in the analysis is to estimate the reference crack opening level. This is achieved by using the method described in previous section as 38. Plot Normalized Stress Versus Normalized COD for second node from the crack tip as shown in Figure 3.9. Then draw a line 1.5% normalized COD value. The intersection stresses are taken as opening and closing level as shown in Figure 3.10. In this analysis a crack advance of $300\mu m$ is considered, as the opening level is stabilized and independent of crack advance as per Figure 3.7.
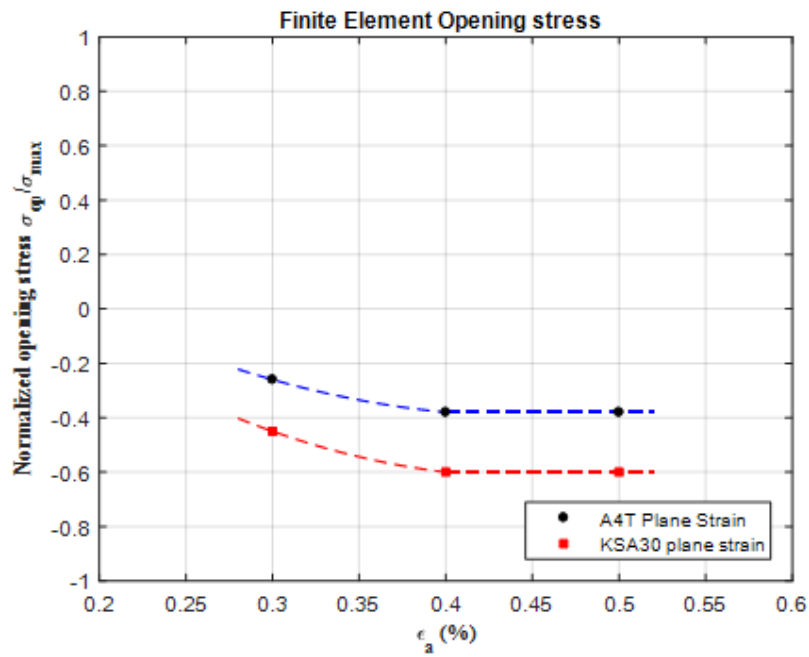
Figure 3.8: Opening Level as a function of Strain Amplitude for A4T and KSA30
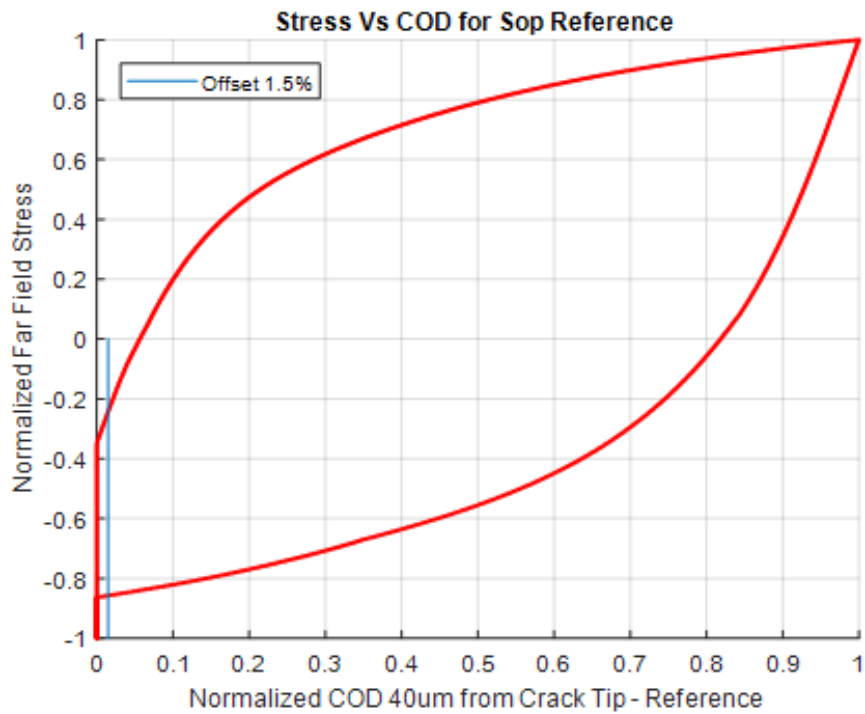
Figure 3.9: Reference Opening Level offset line method
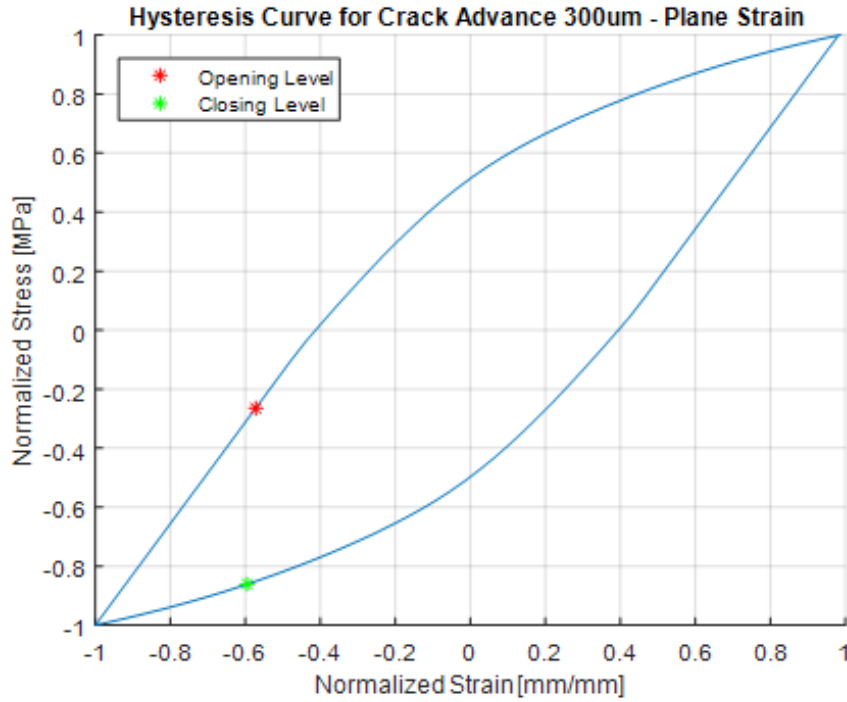
Figure 3.10: Reference Opening and Closing Level

3.4.2 Step 3: Stress Versus COD (Extensometer data from FEM)

First step is to select the plot of Stress Versus COD (Crack Opening Displacement). In DIC it is used $l = 80\mu m$ and $160\mu m$; long virtual extensometer as shown in Figure and distances considered are $d = 60\mu m, 100\mu m,$. So, the normalized stress vs COD plot for the crack advance of $300\mu m$ is as shown in the Figure 3.12.

3.4.3 Step 4: Removing Elastic Part

It can be observed from 3.12 that there is a elastic line in hysteresis curve, this is due to the amount of material above the crack flank and it undergoes some elastic deformation. So, to remove the effect of the material above the crack flank, the elastic part of the COD is removed as shown in Figure 3.13.

3.4.4 Step 4: Offset on Stress Versus Plastic COD

On the stress versus Plastic COD curve, an offset line is drawn whose value has to be identified. This offset line when intersected on the loading curve of plastic COD gives the opening level whose value should be same as that of reference opening level value. Same way, the intersection of this offset line on the unloading curve of the plastic COD gives the closing level whose value should be same as that of reference closing level. This is shown in Figure 3.14.
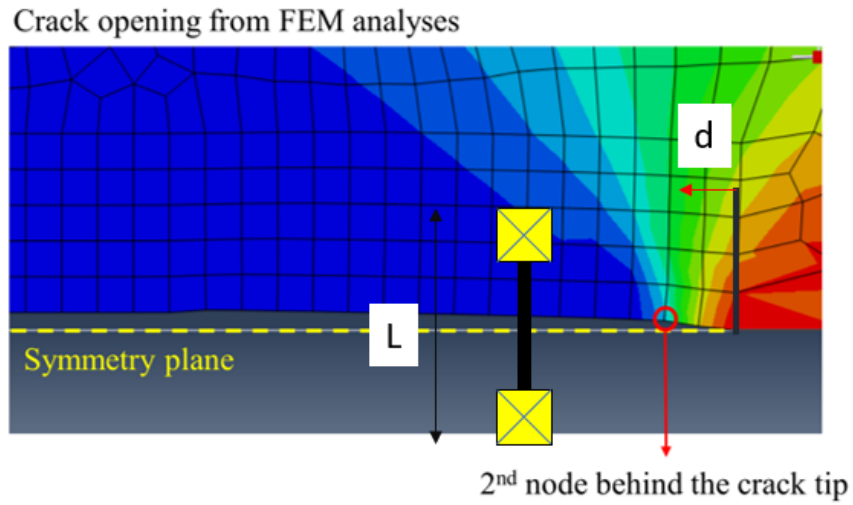
Figure 3.11: Schematic for virtual extensometer in FEM
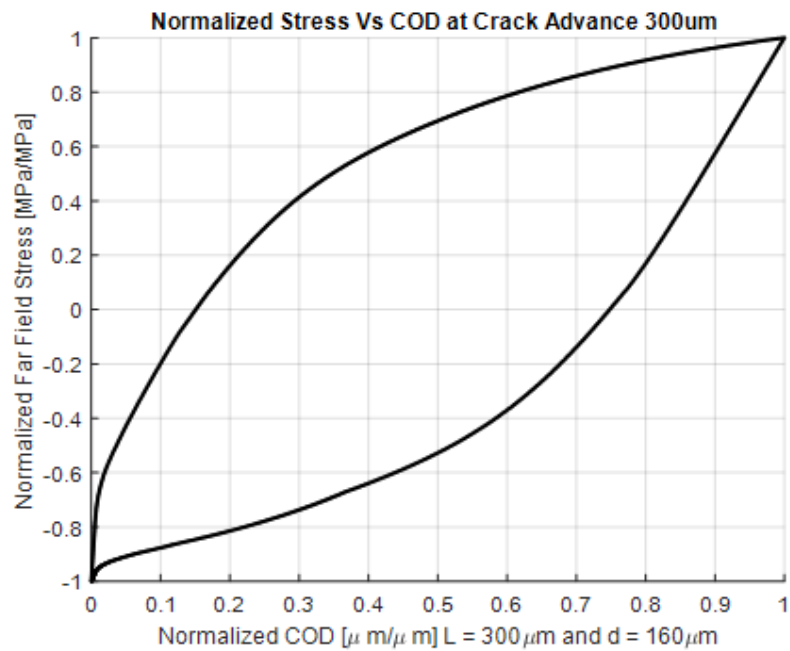
Figure 3.12: Normalized Stress Vs COD at $L = 300\mu m$ and $d = 160\mu m$
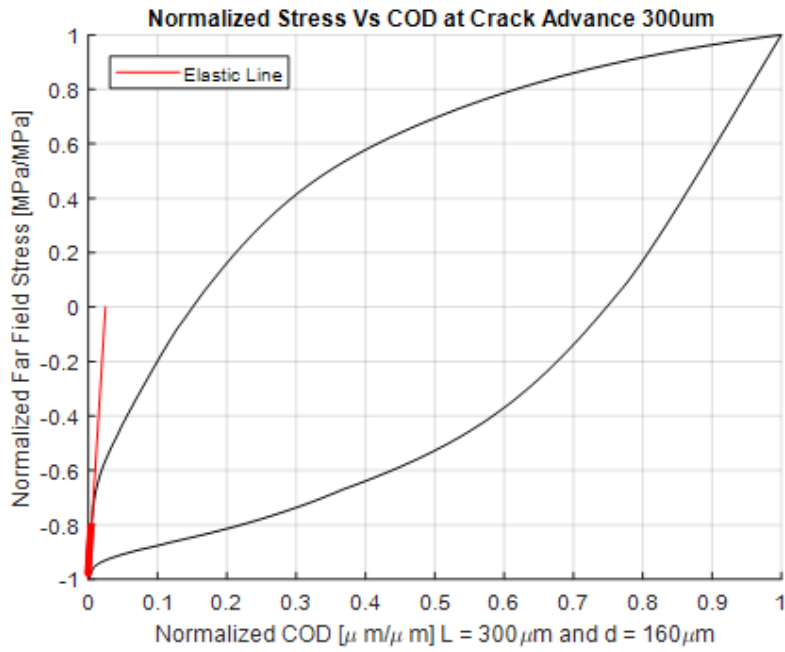
Figure 3.13: Normalized Stress Vs COD at $L = 300 \mu m$ and $d = 160 \mu m$
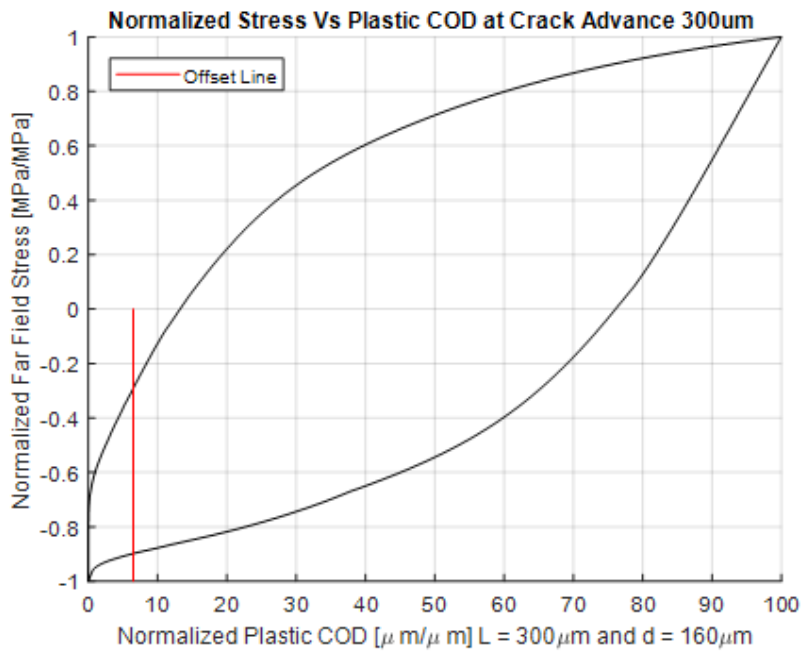
Figure 3.14: Normalized Stress Vs Plastic COD at $L = 300 \mu m$ and $d = 160 \mu m$
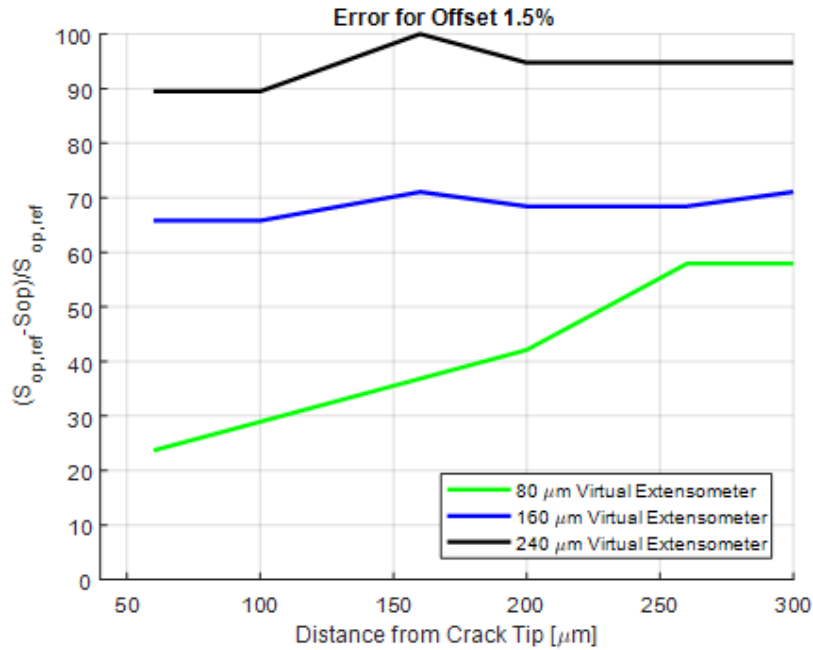
Figure 3.15: Comparison of Offset 1.5% with $S_{op,ref}$

3.4.5 Step 5: Finding the offset Value

In this step, it is required to find the value of offset which gives the same value of reference S_{op}. The analysis was performed with 1.5% offset, 3.0% offset, and 6.5% offset as shown in Figure 3.15,3.16 and 3.17 respectively. It can be observed that for $80\mu m$ extensometer the error is a function of distance from the crack-tip, but for $160\mu m$ extensometer the error is a constant. So, it is recommended to use $160\mu m$ extensometer in DIC virtual extensometer analysis. Referring to Figure 3.17, we can see that for $160\mu m$ extensometer, the estimated opening level is very near to that of the reference opening level (error = 0%). If one use $80\mu m$ extensometer in combination with 6.5% offset, there is a possibility of over-estimating the opening level till $250\mu m$ from the crack tip. It can be seen that higher the length of the extensometer more the elastic part of the COD/Stress loop, so the opening level will lower for same offset value.

3.4.6 Conclusion

From the above analysis, it can be concluded that for DIC measurement of opening level using virtual extensometer, it is recommended to use $160\mu m$ extensometer and a 6.5% offset on the Stress Vs Plastic COD curve.
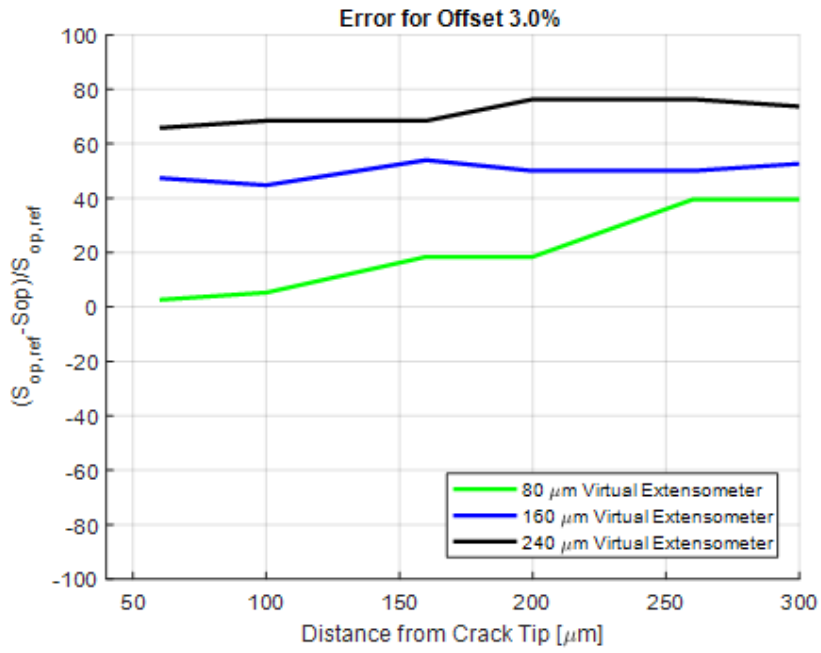
Figure 3.16: Comparison of Offset 3.0% with $S_{op,ref}$
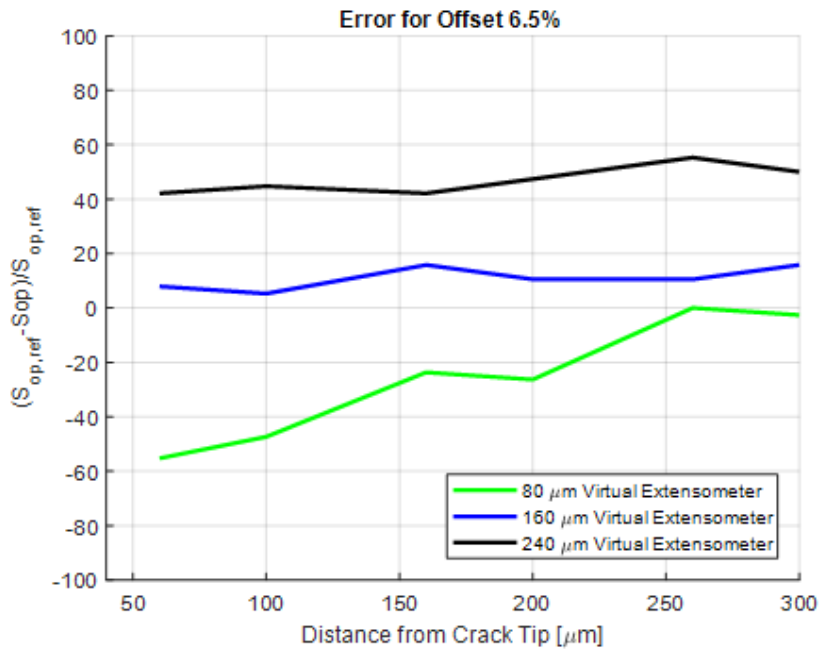
Figure 3.17: Comparison of Offset 6.5% with $S_{op,ref}$
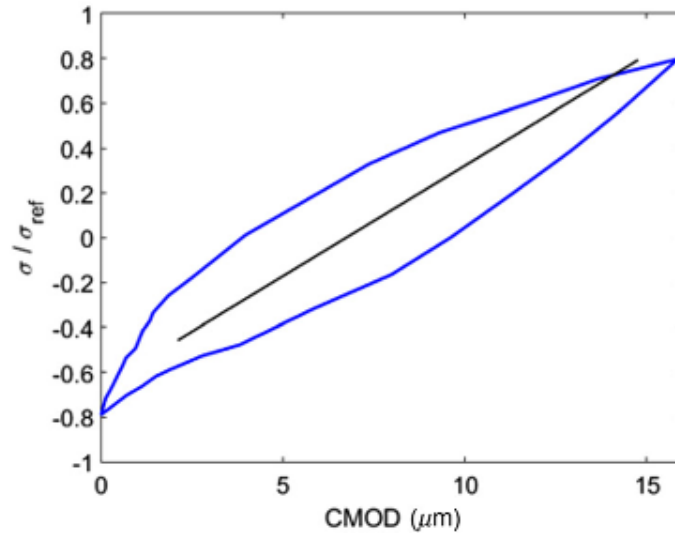
Figure 3.18: Linear COD-Stress fitting

3.5 Comparison of the Offset method with Compliance Offset Method

3.5.1 Overview of Offset Compliance Method

The offset compliance method was employed by Rabbolini [26] in DIC COD versus Stress curve as per [27] and [28]. The method is as follows:

- The part of COD/Stress loop in which loading and unloading branches were not coincident were fitted linearly as shown in Figure 3.18. The linearized COD is represented as:

$$COD_{lin,i} = m\sigma_i + q \tag{3.1}$$

- The offset COD is calculated as shown in Figure 3.19 and is represented by the equation:

$$OffsetCOD_i = COD_i - m\sigma_i - q \tag{3.2}$$

This method was applied to COD/Stress loop of A4T crack propagation at crack advance of 300 μm and results were compared with the offset method developed by the author against the reference opening level by 1.5% offset as shown in Figure 3.20 for 80 μm extensometer and 3.21 for 160 μm extensometer respectively.

From the comparison, we can see that there is a notable amount of variability in the compliance offset results when the COD/Stress loop is noise-free (in this case FEM signal). If there is presence of noise, which can be observed in DIC experiments, the variability of the opening level will be much higher. In compliance offset method, the opening level predicted is higher than the reference opening level at all distances from the crack tip. So, the offset method developed by the author gives much more accurate prediction than the offset compliance method.

Figure 3.19: Offset COD/Stress with Opening Level and Closing Level
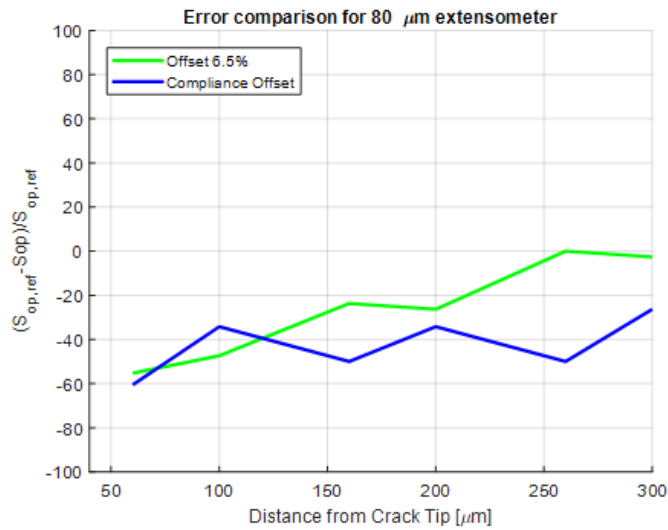
Figure 3.20: 6.5% offset method versus compliance offset method for 80 μm extensometer
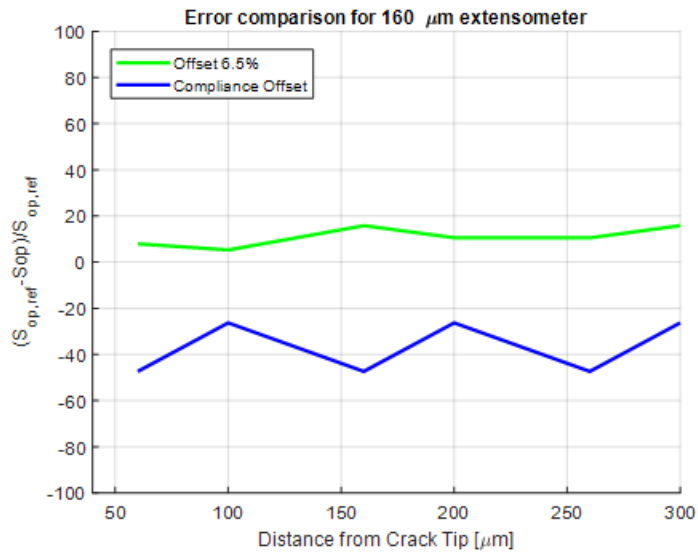
Figure 3.21: 6.5% offset method versus compliance offset method for 160 μm extensometer

3.6 Comparison of the Offset method with Virtual Strain Gauge Method

Another technique used in DIC to measure crack-opening and -closing levels. This is in reference to experiment technique proposed by Vormwald and seeger [20]. In this it was proposed an experimental technique to measure the crack opening level during constant strain amplitude tests on cylindrical specimens. It consists of positioning a strain gauge as near as possible to a fatigue crack. By comparing the stress-strain cycle with the global one, measured by an external extensometer, it is possible to measure crack-opening and -closing levels. Opening and closing levels are estimated as the points in which local and global behavior start to differ. The difference is related to the change of specimen compliance; when the crack flanks are in contact, the zone surrounding the defect behaves in the same way as those zones far from the defect, whereas a loss in local stiffness is measured when the crack starts opening. In particular, when the crack is open, local strains are smaller than the remote ones, because the gauge measures the strain field in the strain shadow of the crack.

This method was tried to implement in the finite element. In analysis, strain was measured at 3 different locations as specified in Rabbolini [26]. The DIC experimental curves are compared against the finite element as shown in Figure 3.22 - 3.24. It can be noted that the averaged strain values of the element shown in the rectangle is taken. From Figure 3.24 it can be seen that the with a change in distance prom the crack tip, the local hysteresis loops are changing considerably. This is in contradiction with the DIC finding. From FEM the mentioned location is the best to measure the averaged strain. The averaged strain values at other locations doesn't give expected local hysteresis loop. This is sensitive to the distance as compared against the DIC. This method is not recommended to use for finding
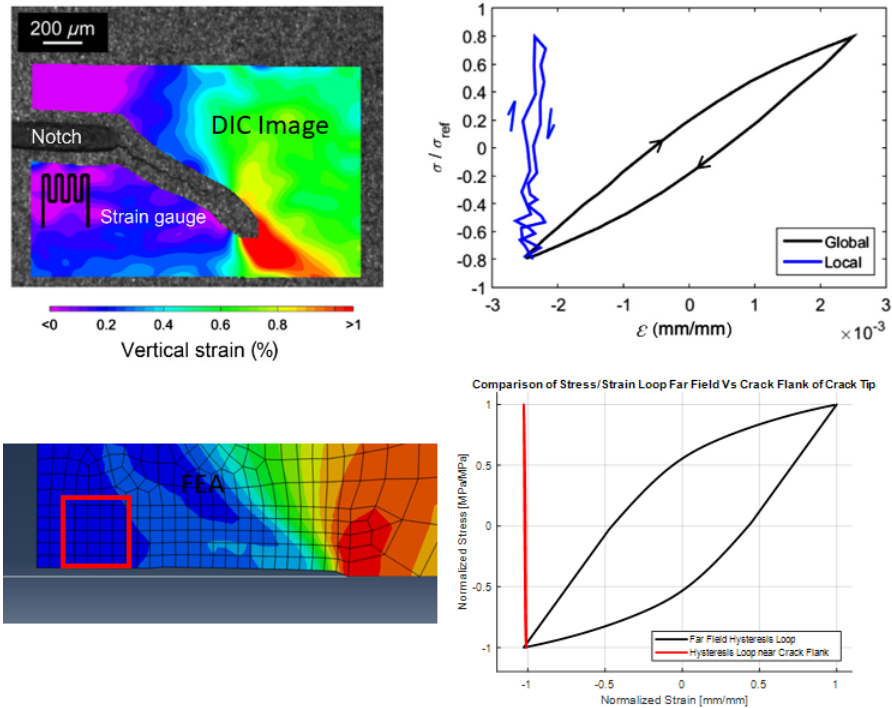
Figure 3.22: Strain Gage Method (Virtual Strain Gage located near the notch)

the opening level in finite element.

3.7 Noise Analysis

Motivation behind this analysis is that from past literatures it was noted that the DIC COD/Stress curves are not smooth as in finite element. It is expected some amount of noise in the signal. Noise can be due to blur in the DIC image or camera is not given enough time to adjust the focus in the DIC video. So, it is required to work on the signal which is having some amount of noise. From previous DIC experimental works it is noted that the signal to noise ratio in the COD signal is approximately 80 dB/sample.

3.7.1 Procedure Adopted for Noise Analysis

The procedure for noise analysis is listed in Figure 3.25. It is seen that the for stress signal the amount of noise is very low (-5 dB/sample). Gaussian noise is added to the signal using awgn() function in MATLAB. The main advantage of this function is that it is only required to specify the signal to noise ratio in dB/sample. Then the noise signal is filtered using median filter so that a new un-noised signal is obtained. This un-noised signal is further processed using offset method to find normalized Sop level. This is useful in analysis the effect of DIC experimental noise on the -opening level.

Figure 3.26 shows for the variability of de-noised COD/Stress loop level in the presence of decreasing noise level (from 75db to 90db). In the cases of higher noise
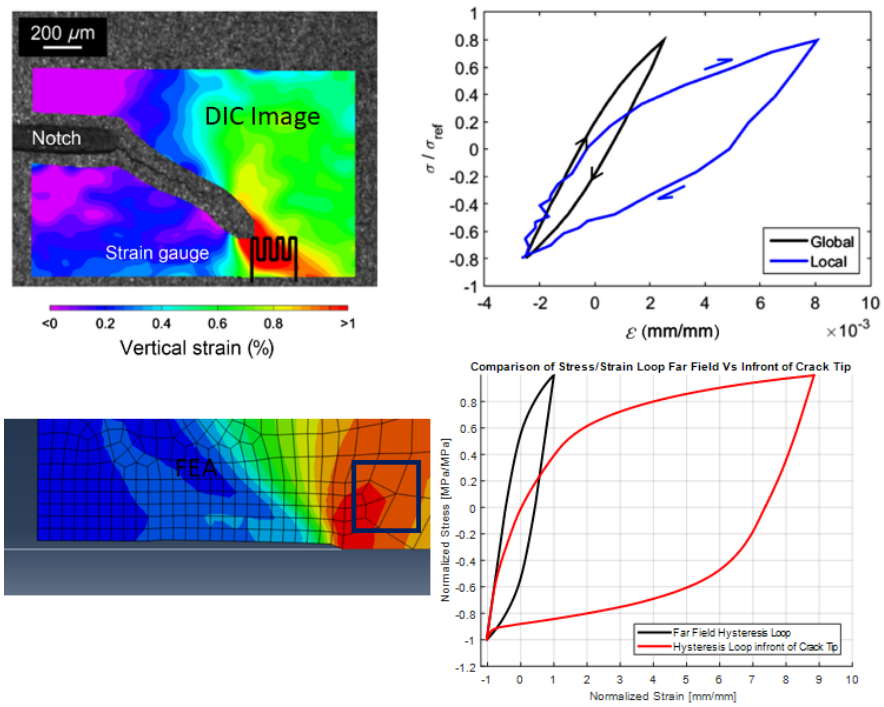
Figure 3.23: Strain Gage Method (Virtual Strain Gage located infront of crack tip above the crack flank)
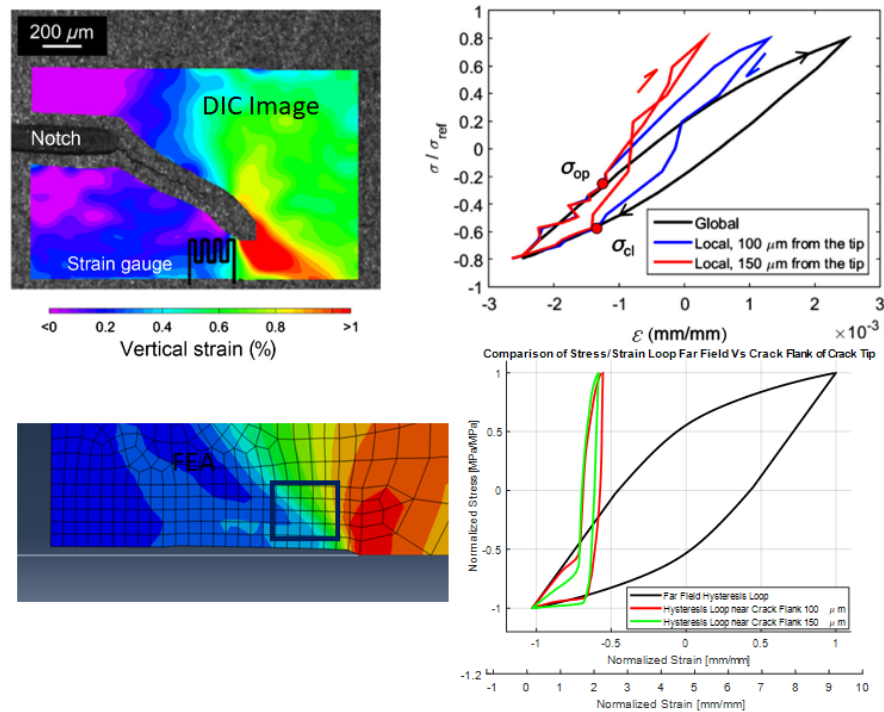
Figure 3.24: Strain Gage Method (Virtual Strain Gage located near the crack flank behind the crack tip)
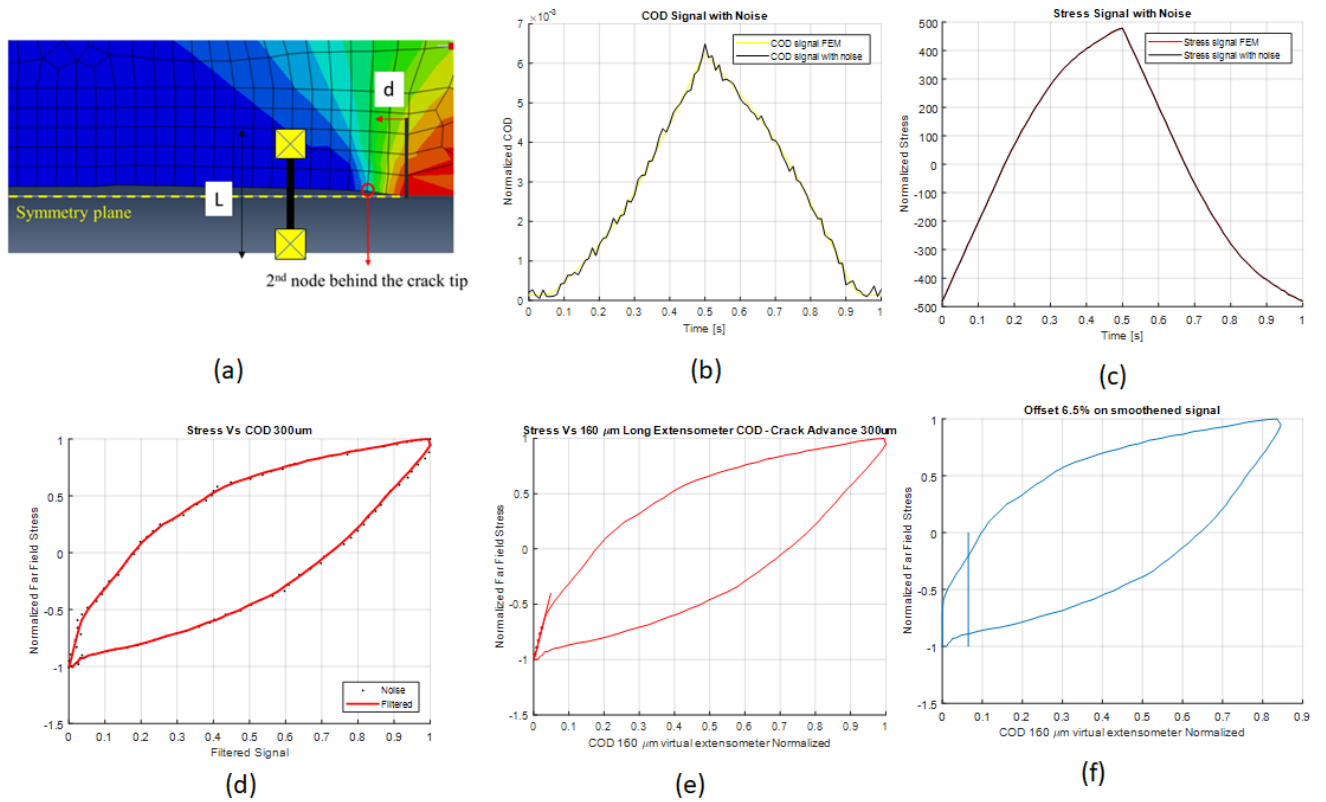
Figure 3.25: (a) Virtual Extensometer 160 μm (b) Addition of noise to COD signal (c) Addition of noise to Stress signal (d) Smoothening of noisy hysteresis loop (e) 6.5% offset to find opening level

signal the de-noised loop is distorted to a high level that the elastic fitting in offset method would become unfeasible and results are not reliable. The variation in the opening level would be higher. So, a statistical method including the noise signal standard deviation is required to be performed.

Figure 3.27 shows the variation of -opening level for increasing distance from the crack tip in 3 different iterations.
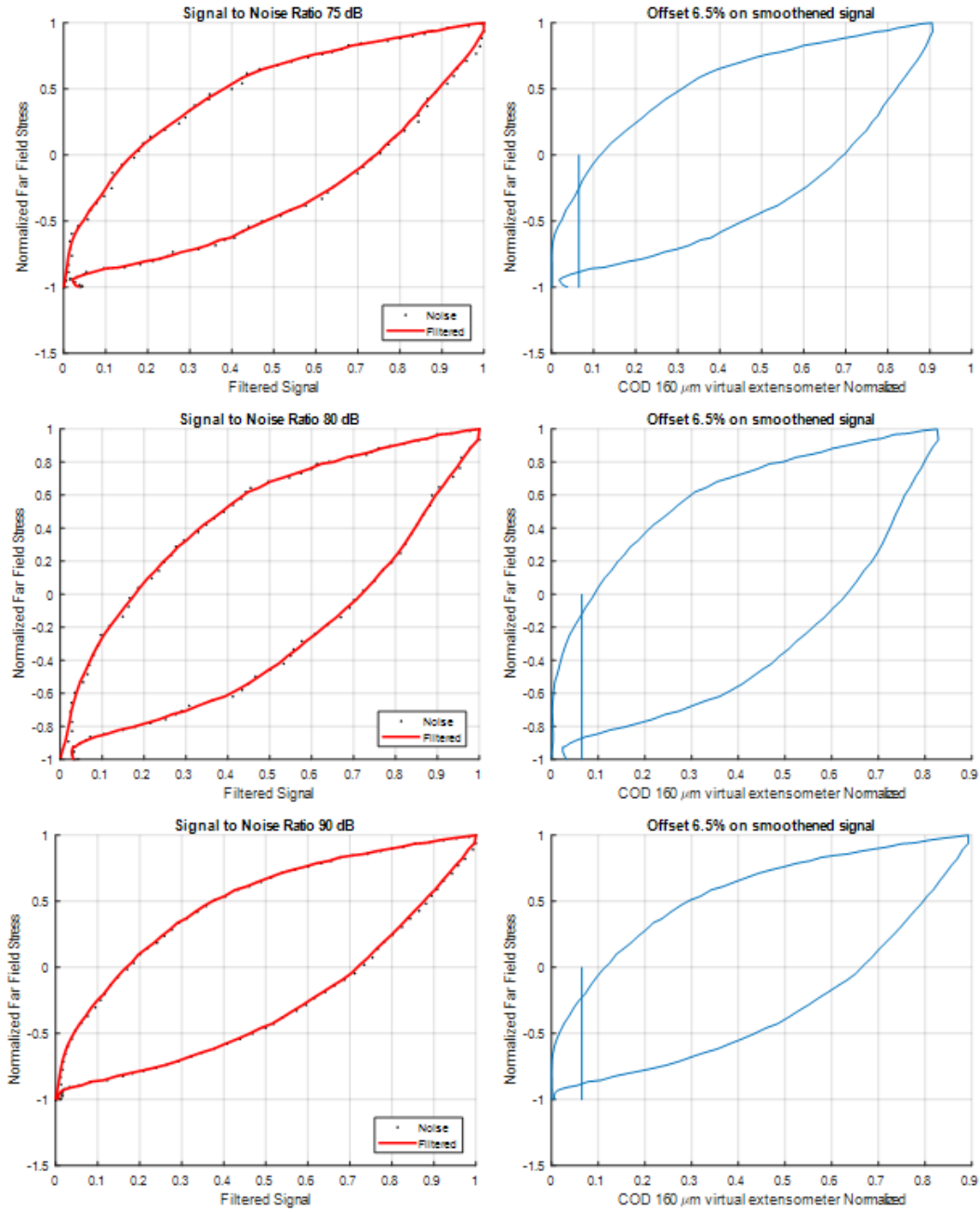
Figure 3.26: Opening level Vs Crack Advance for A4T
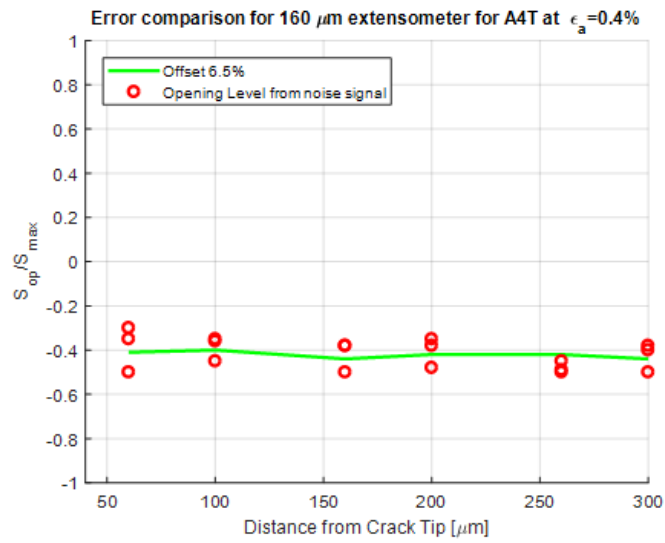
Figure 3.27: Opening level Vs Crack Advance for A4T
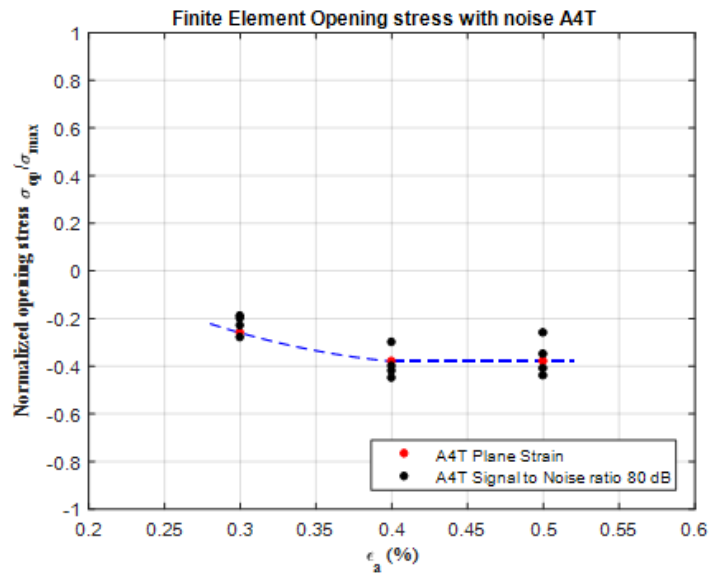
Figure 3.28: Opening level Vs Strain Amplitude for A4T

Chapter 4

Experimental Investigation using DIC

4.1 Introduction to LCF Experiment

After the finite element simulation of LCF crack propagation. The FEM COD vs Stress curves were analyzed, which led to the development of a method to determine crack opening level. Later, expected experimental Gaussian noise was added to FEM signals and analyzed with the developed methods to check the variability of the output. Now an experimental campaign is setup in order to apply the offset method developed by the author. In this chapter, several Low Cycle Fatigue (LCF) tests are conducted in order to study the crack growth phenomenon in the material KSA30.

4.2 Details of the experiment

Low cycle fatigue crack propagation tests were performed at ambient temperature imposing 3 different strain ranges($\Delta\varepsilon_{1,2,3} = 0.3\%, 0.4\%, 0.5\%$). Cylindrical specimen is used in which flat faces are machined on it. It is easy to follow cracks on a planar face than rounded one, since the DIC setup is using only one camera. In order to localize crack growth on a faced specimens, semi-circular defect is introduced through Electro-Discharge Machining with $40\mu m$ radius. The schematic of the specimen is as shown in the Figure 4.1.

Even though, author used A4T and KSA30 for analysis in the previous section, the experiments were performed only on KSA30 due the difficulty in machining the A4T and time availability. All these tests were run controlling the applied strain and imposing a strain ratio R_ε equal to -1. The frequency of loading is 0.5 Hz between the DIC acquisition cycles. After a specified number of cycles, the machine is stopped at zero strain and loading frequency is reduced to 0.05 Hz. This gives 100 DIC images per cycle. But the author decided to lower the loading frequency to 0.02 Hz so that it gives 250 DIC images per cycle. Later part, it can be seen that the noise in the COD/Stress loop is very negligible.

All the tests were performed consistently with the reference standard ASTM E 606 Standard Practice for Strain-Controlled Fatigue Testing [40].
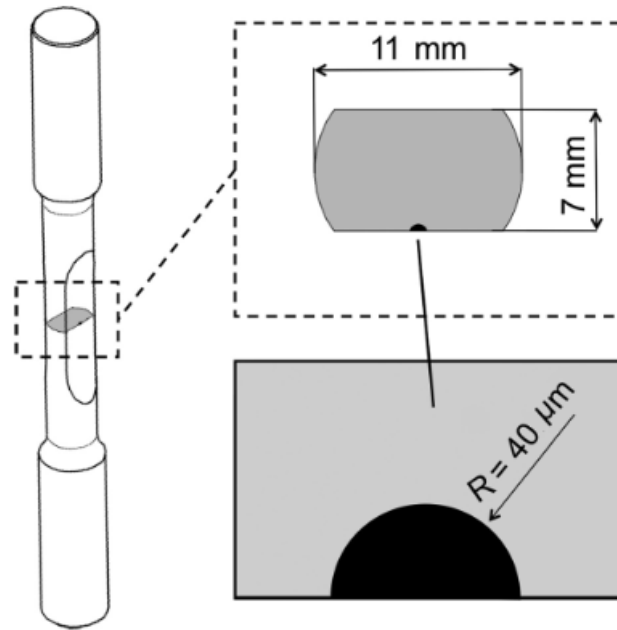
Figure 4.1: Experimental Specimen schematic

All the LCF tests were conducted on a MTS-810 servo-hydraulic testing machine capable of applying a load up to 100 kN available at Politecnico di Milano, Department of Mechanical Engineering. The testing machine alignment was performed as per standard ISO-12106 (*Metallic Materials - Fatigue Testing- Axial-Strain-Controlled Method*) and ASTM E1012 (*Standard Practice for Verification of Test Frame and Specimen Alignment Under Tensile and Compressive Axial Force Application*). All the measurements showed that the bending component is always lower than 5%, as required by the standards.

The experiments were performed with strain-controlled using extensometer. MTS model 632.13F-20 with measurement base (L_0) equal to 10 mm is used.

4.3 Experimental Setup - Digital Image Correlation

4.3.1 Specimen Preparation

The region of the artificial defect becomes the focus region for DIC analysis. The specimen is initially treated with mechanical surface polishing to obtain a polished surface with abrasive paper up to a grit of P2500 as shown in Figure 4.2. Then, a speckle pattern is applied to the specimen surface using black paint by employing an airbrush with a 0.18 mm wide nozzle. All the specimen were painted at the same time as shown in Figure 4.3. This technique allows to have random pattern and it is important to obtain a pattern well distributed on the target surface and the particles have dimension suitable for the magnification to be used in the analysis.
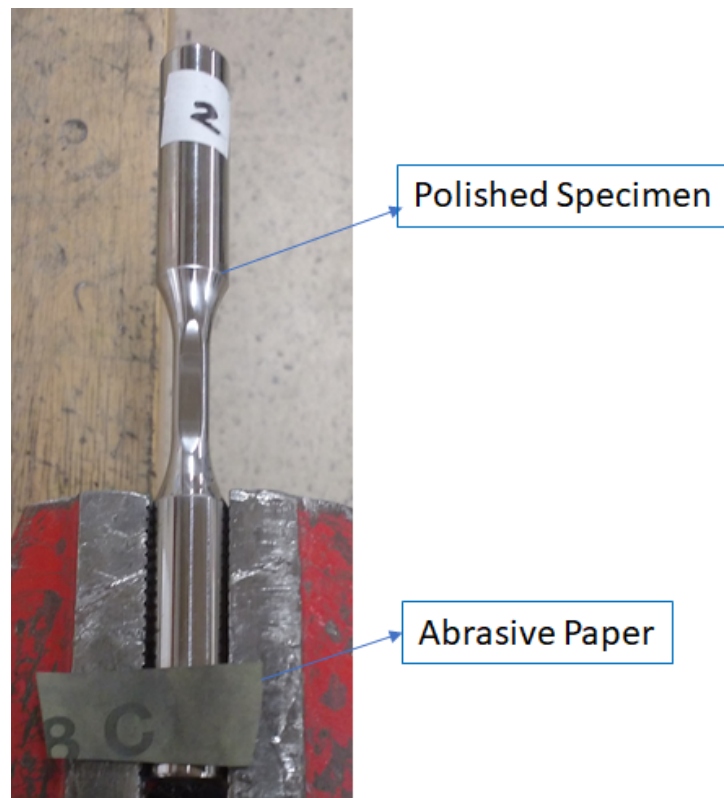
Figure 4.2: Polished Specimen and Abrasive Paper
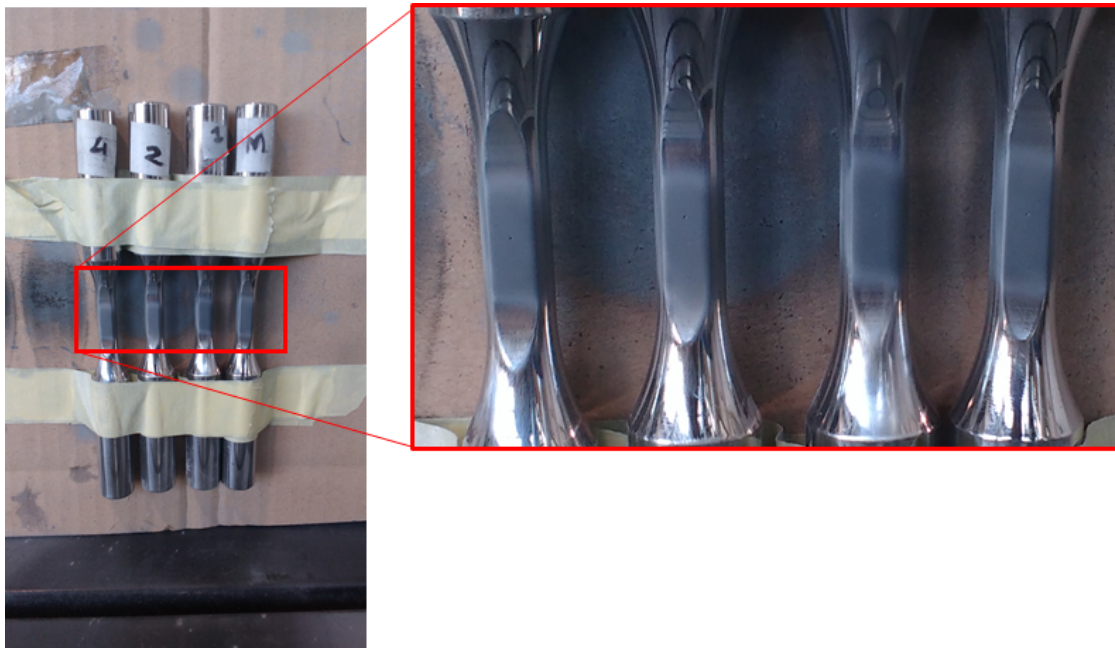
Figure 4.3: Polished Specimen and Abrasive Paper
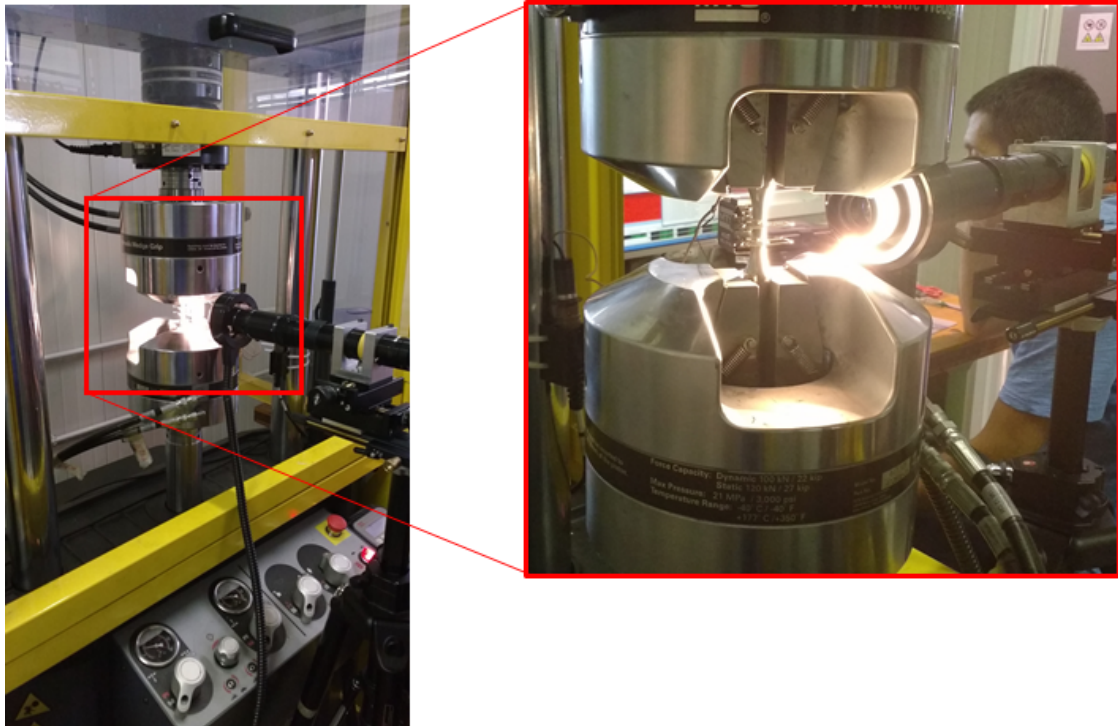
Figure 4.4: Experimental Setup for DIC measurement

4.3.2   Machine Setup

The machine setup is as shown in Figure 4.4. Tests are performed on the test machine described at the initial part of this chapter and employing a camera for image acquisition. The acquisition set is composed by a digital camera Allied Vision Manta G20B with 2 megapixel. The optics are produced by Optem which is composed of lens allowing 10x magnification with the flexibility of additional magnification up to 6.5x. Around the optics an annular LED light is placed to obtain a parallel beam and uniform light distribution on the target surface in the acquisition time. The acquisition system is placed on a support that is able to translate in three cartesian cordinate direction (x,y,z):

- x_i defined as the direction camera-specimen, allowing to adjust the focus;

- y_i defined as the horizontal perpendicular to x, allow to follow the crack when it oversteps the limits of the analyzed region;

- z_i defined as the vertical direction, it allows to adjust the height of the camera with respect to the artificial defects/a defected crack.

By means of a Labview software the images are acquired automatically during the cycle, concomitant with the acquisition of stresses and strains measured by the load cell and the extensometer. Usually the acquisition was set to obtain 100 frames per cycle. But in this case, it was decided to use 250 frames per cycle. The reason behind this was to reduce the noise in the DIC acquisition. Lower the loading frequency, better the time allowed to adjust the focus by the camera. So, this leads to a better clarity of the DIC images acquired.
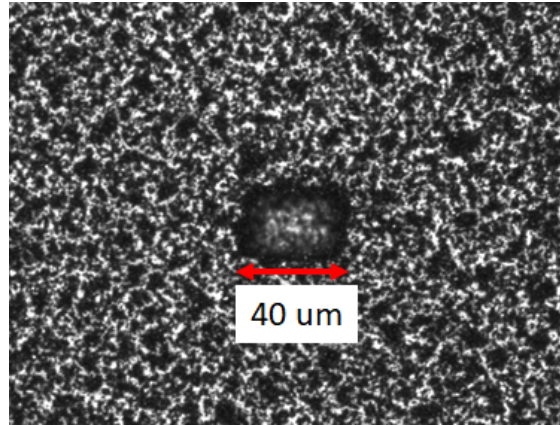
Figure 4.5: Speckle pattern
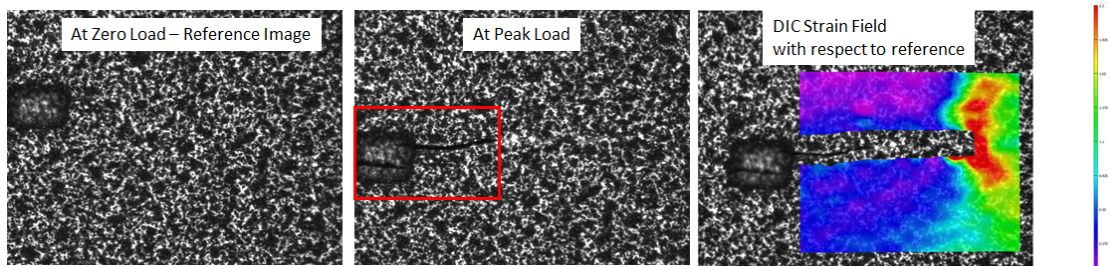
Figure 4.6: Strain Field using DIC 2D

4.4 Experiment Procedure with DIC

The DIC camera is setup and focused on the EDM notch in order to capture the reference image. The speckle pattern is as shown in Figure 4.5. DIC compares the other images with the reference image, this is a significant step in the experiment. Now the specimen is cycled at 0.5 Hz through the desired strain amplitude, till the crack start to propagate slowly. After some specified cycle (for example 200 cycle for strain amplitude 0.5%), the machine is stopped and the frequency of loading is changed to 0.02 Hz. The specimen is loaded for 3-4 cycles and one complete cycle is captured using the camera. Then the loading is continued at 0.5 Hz for next specified number of cycle. This process is continued till crack reaches a length of approx. 2.5 mm to 3 mm.

4.5 Analysis of the experimental Results

The DIC 2D software compares, the 250 images acquired in one cycle against the reference images to give the strain field as shown in the Figure 4.6. It can be noted that the crack is fully open at peak load and the strain field in front of crack tip. Even though the peak load image is displaced with respect to reference image, the user manually provides the initial guess for subset matching in DIC 2D software so that the software makes the computation for the strain field. The subset size used is 81 pixels.

For each strain amplitude, DIC analysis was performed. The figure shows the
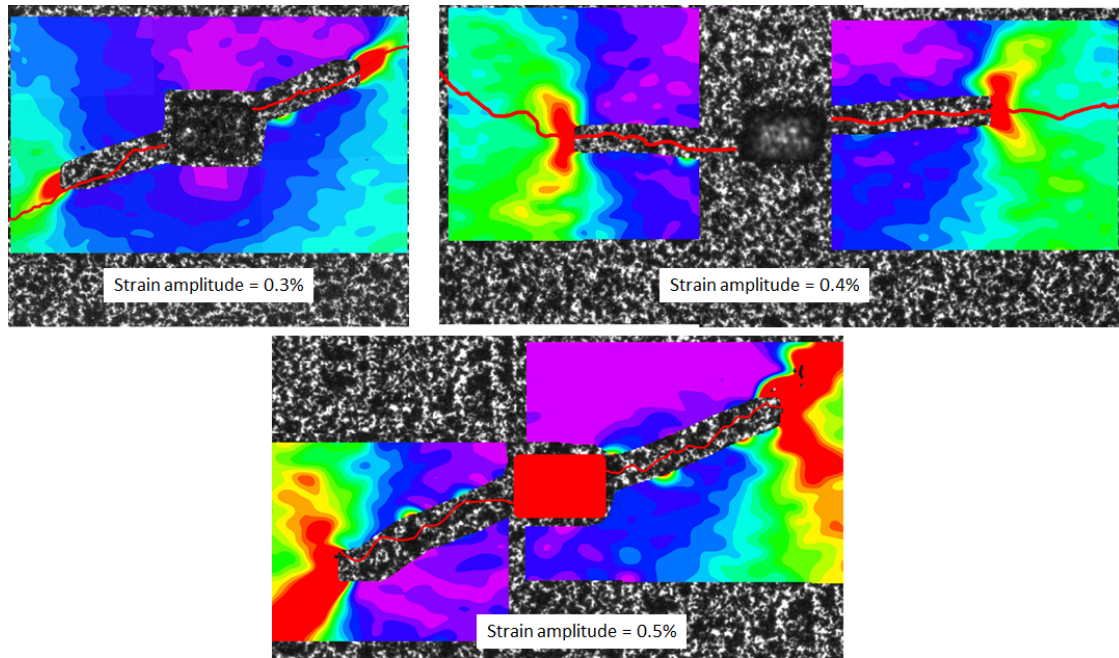
Figure 4.7: Strain Field using DIC 2D

final crack shape and the strain field for each strain amplitude is shown in Figure 4.7.

4.5.1 Opening Level using Virtual Extensometer

In this section, the author will use the virtual extensometer to measure the crack opening displacement and it is plotted against the stress. The offset method developed in the previous chapter will be used to determine the crack opening level.

- The virtual extensometer of 160-170 μm is placed on the crack as shown in the Figure 4.8(a). The length of the extensometer is already decided from the previous analysis in the last chapter.

- Once the extensometer time history is extracted, it is plotted against the stress to obtain COD/Stress loop as shown in Figure 4.8(b). It can be noted that the there is an elastic part due to the material between the extensometer and the crack flank. The elastic lines are plotted.

- Now the elastic part is removed from the COD/Stress loop to obtain plastic COD/Stress loop and a vertical offset of 6.5% is drawn as shown in Figure 4.8(c). The intersection of the offset line with loading part of the plastic COD/Stress loop gives the opening stress level.

- Figure 4.8(d) shows the opening stress level on the stress-strain hysteresis loop of the KSA30 specimen.

In this analysis it can be seen that the COD/Stress curve is very smooth, more similar to the FEM curve. Thanks to decreasing the loading frequency during the
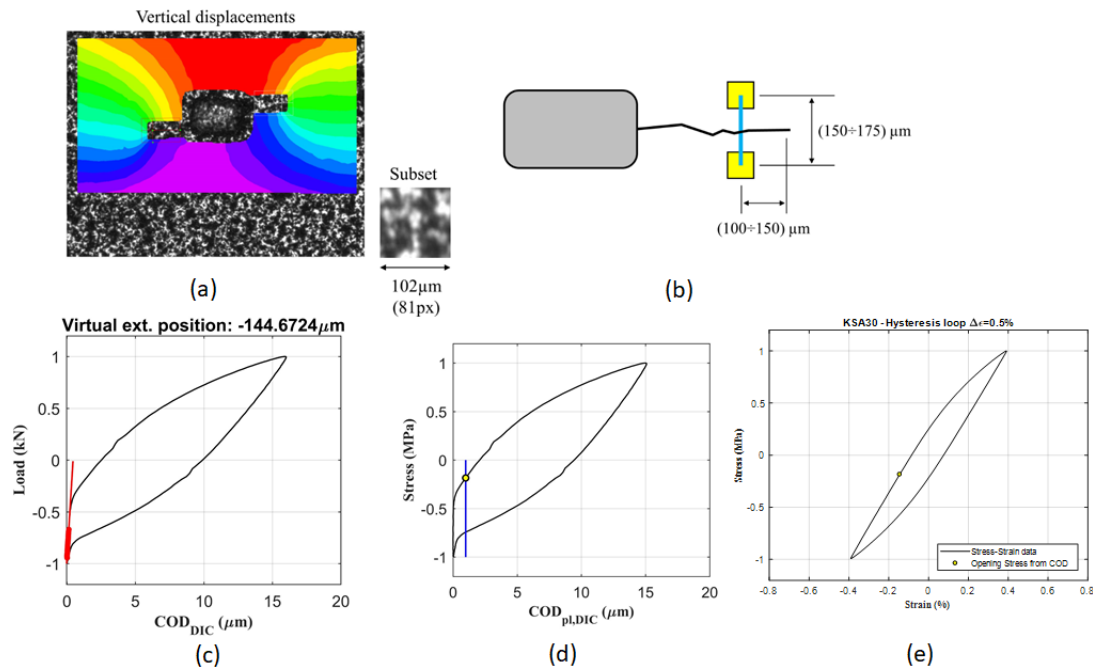
Figure 4.8: Offset Analysis in DIC

acquisition from 0.05 Hz (100 images/cycle) to 0.02 Hz (250 images/cycle). The different in noise level can be compared against the work of Rabbolini and the current experiment as shown in Figure 4.9.

4.5.2 Opening Level Results

The DIC opening level results are plotted in Figure 4.10 for different crack lengths. From the plot it can be seen that for $\varepsilon_a = 0.3\%$, the opening level is very near to zero and this the expected behavior of this particular type of steel. So, the offset value of 6.5% is a simple and robust method to determine the opening stress level.

The opening level for different strain amplitudes are plotted in Figure 4.11. It can be seen the trend of decrease in opening level when the strain amplitude is increased. This trend is same in DIC experiment and FEM. But the opening level of FEM is very lower to that of DIC opening level. One of the possible explanation to this may lie in the experimental investigation used to determine the material model for KSA30. The maximum strain amplitude at which the LCF experiment was done is 0.80%. But during crack propagation, the strain in front of crack tip can go to the range of 5 to 6%. But the model parameter is valid for upto 0.8% and it can be extrapolated with a good accuracy till 1.5%. Above that, the extrapolation may not be accurate and it affects the opening level. So, it is required to identify the model parameters for a strain amplitude of 1.5% to 2.0% which has been already done for A4T.

Second explanation may be the number of cycle between each node release. In this thesis, 2 cycles between the node release is used which may not be enough to match the strain field of the experiment with the FE Plane Strain. More cycles

(a) 100 images/cycle　　　　(b) 250 images/cycle
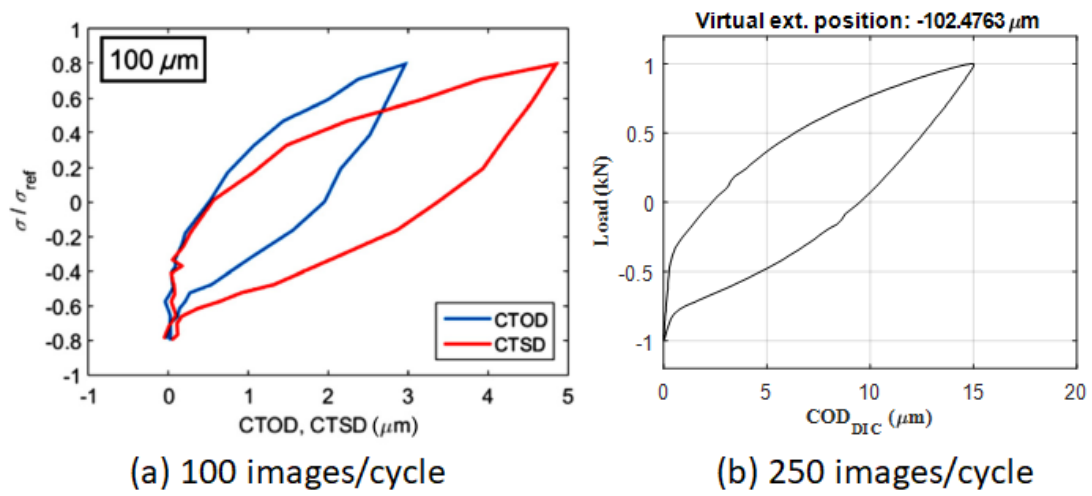
Figure 4.9: Comparison of Noise (a) 100 images/cycle (Source [26]) and (b) 250 images/-cycle
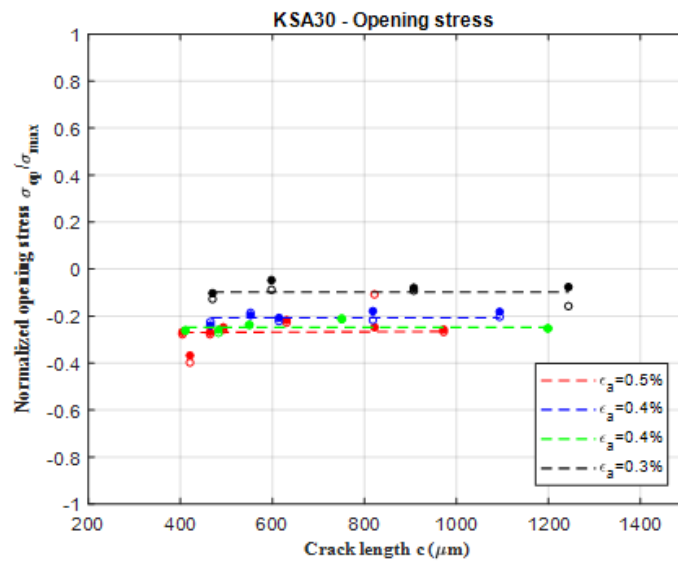
Figure 4.10: Opening Level versus Crack Length (for different ε_a)
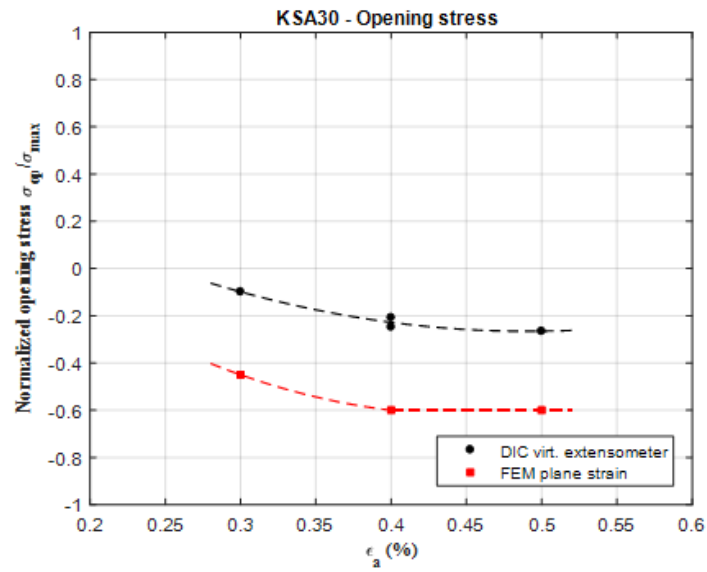
Figure 4.11: Opening Level versus Strain Amplitude (Experimental and FEA)

between the node release may help to match the strain field of experiment and ultimately we can predict FEM opening level with considerable accuracy. The effect of number of cycles between node release needs to be verified in the future work.

Conclusion

The aim of this thesis work was the development of simple and robust method which can be used to calculate the opening level from DIC virtual extensometer with considerable accuracy. Before finalizing this offset method, several issues were encountered related to the development of the model for A4T and KSA30. The deep knowledge of crack opening and closing behavior helped to assess the results of finite element simulations.

In this thesis, the systematic study of all the previous works done on Low Cycle Fatigue crack opening level is conducted. All the experimental methods to measure crack opening level is chronologically recorded. There exists a very few finite element study on crack closure in Low cycle fatigue, which is explained in the literature review. To simulate crack closure it is required to identify the parameters for Chaboche model. Since the this model is complex compared to the models used in the past literatures, good amount of time is invested in programming. This helped the author in simulating the crack propagation at higher strain amplitudes. The finite element signals from the simulation were analyzed to develop the offset method. This method were compared against previous existing methods like virtual strain and compliance offset method. The length of the virtual extensometer to be used in the experiment is determined.

The DIC Low cycle fatigue experiment is performed on the 4 specimens of KSA30. Noise in the COD/Stress graph was expected. Due to the use of lower frequency of loading during acquisition, the noise in the results were reduced by significant amount. The offset method were used and opening level were determined from DIC results. There is a considerable difference between the experimental and FE Plane Strain result. Possible reasons were hypothesized. In future, DIC experiment needs to be performed on the material A4T and opening levels have to be found out using offset method. Also, further experiments needs to be conducted on KSA30 at higher strain amplitude for the identification of Chaboche parameters. This may help to correct the difference in the experimental and FE Plane Strain opening levels.

Appendix A

MATLAB CODES

A.1   Isotropic Hardening Parameter using Least Square Fitting in MATLAB

```matlab
% Caculation of all 3 Isotropic Hardening Parameters
    using Least Square Fitting
C_inf_mat = zeros(6,1);
b_mat = zeros(6,1);
sig_0_mat = zeros(6,1);
data = load('MO64AR-1.mat');
for i=1
iso_data = data.SPECIMEN(i).S0;
sig0_exp = iso_data(2,2:end);
plstr = iso_data(1,2:end);
sig0_end = iso_data(2,end);
sig_0 = iso_data(2,2);
figure(i);
hold on;
%grid on;
plot(iso_data(1,:),iso_data(2,:));
F = @(x,xdata)(x(1)*(1-(exp(-x(2)*xdata)))+x(3));
x0 = [-50 1.5 242];
[x,resnorm,~,exitflag,output] = lsqcurvefit(F,x0,plstr,
    sig0_exp);
plot(plstr,F(x,plstr))
xlabel('Cumulated Plastic Strain \epsilon_{pl}');
ylabel('Yield stress \sigma_{0}');
title('Isotropic Hardening Curve');
sig0_th = x(3)+x(1)*(1-exp(-x(2)*plstr));
hold on;
plot(plstr,sig0_th,'LineWidth',2);
C_inf_mat(i) = x(1);
b_mat(i) = x(2);
```

```matlab
29 sig_0_mat(i) = x(3);
30 legend('Experimental','Isotropic Model Fitting');
31 end
32
33 C_inf_avg = sum(C_inf_mat)/i;
34 b_mat_avg = sum(b_mat)/i;
35 sig_0_avg = sum(sig_0_mat)/i;
```

A.2   Kinematic Hardening Hardening Parameter using Least Square Fitting in MATLAB

```matlab
1  clear all
2  close all
3  clc
4
5  % Loading data
6  data = load('M064AR-1.mat');
7  HYS = load('Hyst_1.mat');
8  n = 6;
9  %Kinematic hardening parameters for Specimen 1
10 sigma0_end= data.SPECIMEN(1).S0(2,end);
11 Stress = HYS.Hyst_1(:,2);
12 Strain = HYS.Hyst_1(:,1);
13 %Fitting for Elastic Modulus
14 p3= polyfit(Strain(1:35),Stress(1:35),1);
15 r3= polyval(p3,[-0.007:0.0001:0.0]);
16 E_stab= p3(1);
17 stabilizedPlasticStrain= Strain-Stress./E_stab;
18 dim= [20 16];
19 fig= figure('PaperPosition', [0 0 dim],'PaperSize',dim);
20 plot(Strain,Stress,'b','LineWidth',1.5)
21 hold on;
22 plot([-0.007:0.0001:0.0],r3,'r--','Linewidth',1.5);
23 %grid;
24 xlim([-0.01 0.01])
25 ylim([-500 500])
26 xlabel('Strain \epsilon [mm/mm]')
27 ylabel('Strain \sigma [MPa]')
28 hold off
29 print(fig,'StabIsteresisLoop','-dpdf');
30 x_interp= [-0.005:0.0001:-0.002];
31 y_interp= ones(1,length(x_interp))*(2*sigma0_end)+min(
       Stress);
32 sigma1= Stress(50);
33 epsilon1=stabilizedPlasticStrain(50);
```

```matlab
34 | fig= figure('PaperPosition', [0 0 dim],'PaperSize',dim);
35 | plot_1= plot(stabilizedPlasticStrain,Stress,'b','
     | LineWidth',1.5);
36 | hold on;
37 | plot_2= plot(stabilizedPlasticStrain,Stress,'b','
     | LineWidth',1.5);
38 | plot_3= plot(x_interp,y_interp,'r--','LineWidth',1.5);
39 | plot_4= plot(epsilon1,sigma1,'r.','MarkerSize',20);
40 | %grid;
41 | xlim([-0.01 0.01])
42 | ylim([-500 500])
43 | xlabel('Plastic Strain \epsilon_{pl} [mm/mm]')
44 | ylabel('Stress \sigma [MPa]')
45 | legend([plot_1 plot_4],'Hysteresis loop','(\sigma_{1},\
     | epsilon_{1})','Location','SouthEast')
46 | hold off
47 | print(fig,'Sigma1Epsilon1Chart','-dpdf');
48 | yK= Stress(50:end)-sigma0_end;
49 | y1= sigma1-sigma0_end;
50 | xdata1 = stabilizedPlasticStrain(50:end)-
     | stabilizedPlasticStrain(50);
51 | F = @(x,xdata)((x(1)/(5700)).*(1-exp(-(5700)*xdata))+(y1
     | /3).*exp(-(5700)*xdata)+...
52 | (x(2)/(600)).*(1-exp(-(600)*xdata))+(y1/3).*exp(-(600)*
     | xdata)+...
53 | (x(3)/0.001).*(1-exp(-0.001*xdata))+(y1/3).*exp(-0.001*
     | xdata));
54 |
55 | x0= [600000 80000 6000];
56 | [x,resnorm,~,exitflag,output] = lsqcurvefit(F,x0,xdata1,
     | yK);
57 | fig = figure('PaperPosition', [0 0 dim],'PaperSize',dim)
     | ;
58 | plot(xdata1,yK,'k','LineWidth',2);
59 | hold on
60 | plot(xdata1,F(x,xdata1),'r','LineWidth',1.0);
61 | %grid
62 | xlim([-0.002 0.008])
63 | ylim([-800 800])
64 | xlabel('\epsilon_{pl}-\epsilon_{pl}^{1} [mm/mm]')
65 | ylabel('\sigma-\sigma_{0} [MPa]')
66 | legend('Experimental curve','Interpolating curve N=3','
     | Location','SouthEast')
67 | hold off
68 | print(fig,'Interpolation2','-dpdf');
```

A.3 Noise analysis on Virtual Extensometer COD/Stress Loop

```matlab
clear all
close all
clc

data = load('Data.txt');
for i=5
%start = 2000;
start = 156;
fin = 256;
figure();
hold on;
grid on;
COD = data(start:fin,i+4);
Stress = data(start:fin,4);
noise_COD = awgn(COD,70);
noise_Stress = awgn(Stress,-5);
time = data(start:fin,1)-min(data(start:fin,1));
plot(time,COD,'y');
plot(time,noise_COD,'k');
xlabel('Time [s]');
ylabel('Normalized COD');
title('COD Signal with Noise');
legend('COD signal FEM','COD signal with noise');


figure();
hold on;
grid on;
plot(time,Stress,'r');
plot(time,noise_Stress,'k');
xlabel('Time [s]');
ylabel('Normalized Stress');
title('Stress Signal with Noise');
legend('Stress signal FEM','Stress signal with noise');

figure();
hold on;
grid on;
plot(noise_COD/max(noise_COD),noise_Stress/max(
    noise_Stress),'r');
xlabel('Normalized COD 40um from Crack Tip - Reference')
    ;
```

```matlab
42  ylabel('Normalized Far Field Stress');
43  title('Stress Vs COD for Sop Reference');
44
45  figure();
46  hold on;
47  grid on;
48  COD_Smooth= medfilt1(noise_COD,4);
49  COD_Smooth1=COD_Smooth(1:51);
50  COD_Smooth2=COD_Smooth(52:end);
51  pp_COD1 = csaps(time(1:51),COD_Smooth1,0.99999,time
       (1:51));
52  pp_COD2 = csaps(time(52:end),COD_Smooth2,0.99999,time
       (52:end));
53  pp_COD = cat(1,pp_COD1,pp_COD2);
54  Stress_Smooth = medfilt1(noise_Stress,1);
55  Stress_Smooth1=Stress_Smooth(1:51);
56  Stress_Smooth2=Stress_Smooth(52:end);
57  pp_Stress1 = csaps(time(1:51),Stress_Smooth1,1,time
       (1:51));
58  pp_Stress2 = csaps(time(52:end),Stress_Smooth2,1,time
       (52:end));
59  pp_Stress = cat(1,pp_Stress1,pp_Stress2);
60  plot(time,(COD_Smooth-min(COD_Smooth))/(max(COD_Smooth)-
       min(COD_Smooth)),'.');
61  plot(time,(pp_COD-min(pp_COD))/(max(pp_COD)-min(pp_COD))
       ,'r','LineWidth',2);
62  xlabel('Time [s]');
63  ylabel('Normalized COD');
64  title('Filtered COD Signal');
65
66  figure();
67  hold on;
68  grid on;
69  plot(time,Stress_Smooth/max(Stress_Smooth),'.');
70  plot(time,pp_Stress/max(pp_Stress),'r','LineWidth',2);
71  xlabel('Time [s]');
72  ylabel('Normalized Stress');
73  title('Filtered Stress Signal');
74
75  figure();
76  hold on;
77  grid on;
78  start = 1;
79  fin = length(pp_COD);
80  plot((COD_Smooth(start:fin)-min(COD_Smooth(start:fin)))
       /(max(COD_Smooth(start:fin))-min(COD_Smooth(start:fin
       ))),Stress_Smooth(start:fin)/max(Stress_Smooth(start:
```

```matlab
      fin)),'.k');
81 plot((pp_COD(start:fin)-min(pp_COD(start:fin)))/(max(
      pp_COD(start:fin))-min(pp_COD(start:fin))),pp_Stress(
      start:fin)/max(pp_Stress(start:fin)),'r','LineWidth
      ',2);
82 xlabel('Filtered Signal');
83 ylabel('Normalized Far Field Stress');
84 title('Signal to Noise Ratio 90 dB');
85 legend('Noise','Filtered','Location','SouthEast');
86
87 figure();
88 hold on;
89 grid on;
90
91 COD = (pp_COD(start:fin)-min(pp_COD(start:fin)))/(max(
      pp_COD(start:fin))-min(pp_COD(start:fin)));
92 P = pp_Stress(start:fin)/max(pp_Stress(start:fin));
93 plot(COD,P,'-r');
94
95 xlabel('COD 160 \mum virtual extensometer Normalized');
96 ylabel('Normalized Far Field Stress');
97 title('Stress Vs 160 \mum Long Extensometer COD - Crack
      Advance 300um');
98
99 lim_up = -0.98*(max(P));
100 lim_down = -0.7*max(P);
101 indx = find(P(1:51)>lim_up & P(1:51)<lim_down);
102 plot(COD(indx),P(indx),'or','LineWidth',1.5,'MarkerSize
      ',2,'MarkerFaceColor','r'); hold on; grid on;
103
104 p_op_com = polyfit(COD(indx),P(indx),1);
105 Px = -1:0.01:-0.4;
106 CODy = (Px-p_op_com(2))./p_op_com(1);
107 open_comp = p_op_com(1);
108 plot(CODy,Px,'-r','LineWidth',1.0); hold on; grid on;
109
110 COD_pl = COD-P/p_op_com(1);
111 figure();
112 hold on;
113 grid on;
114 xlabel('COD 160 \mum virtual extensometer Normalized');
115 ylabel('Normalized Far Field Stress');
116 title('Offset 6.5% on smoothened signal');
117 plot(COD_pl-min(COD_pl),P,'-','LineWidth',1.0);
118 line([0.065 0.065],[-1.0 0]);
119 end
```

Bibliography

[1] W.Elber. *Fatigue crack growth under cyclic tension.* Engineering Fracture Mechanics, 2(1):37-45,1970.

[2] W.Elber *The significance of fatigue crack closure.* In Damage tolerance in air craft structures, ASTM STP 486, pages 230-242.American society for Testing and Materials,1971.

[3] Ji-Ho Song, Jae-Youn Kang, and Ja-Suk Koo. *Proposal of modified (normalized) ASTM offset method for determination of fatigue crack opening load.* International Journal of Fatigue ,27(3):293-303,2005.

[4] McEvily,A.J.(ASTM International,1988) *On crack closure in fatigue crack.* in STP 982 Mechanics of Fatigue Crack Closure 35-43

[5] Louat, N.,Sadananda, K.,Duesbery,M and Vasudevan, A.K. (1993) *A theoretical evaluation of crack closure.* Metallurgical Transactions A, **24**,2225-2232.

[6] Vasudevan, A.K. (1993),Sadananda, K.,Louat, N., *A review of crack closure, fatigue crack threshold and related phenomena.* Materials Science and Engineering A,**188**,1-22

[7] Zhang, C., Marissen, R., Schulte, K., Trautmann, K.H., Nowack, H., and Schijve,J., *Crack Propogation Studies on Al 7475 on the Basis of Constant Amplitude and Selective Variable Amplitude Loading Histories.* 1985

[8] K.J Miller. *Materials science perspective of metal fatigue resistance.* Material science and technology, 9(6):453-462,1993.

[9] J.R Rice *A path independent integral and the approximate analysis of strain concentration by notches and cracks.* Journal of Applied Mechanics, 35:379-386, 1968.

[10] N.E. Dowling. *Cyclic Stress-Strain and Plastic Deformation Aspects of Fatigue Crack Growth.* ASTM,1977.

[11] N.E. Dowling and J.A. Begley. Fatigue crack growth during gross plasticity and the J-Intergral. In *Mechanics of crack growth*, pages 82-103. ASTM, 1976

[12] J.C. Newman Jr. A finite element analysis of fatigue crack closure. In *Mechanics of crack growth, ASTM STP 590*, pages 281-301. American Society for Testing and Materials, 1976

[13] H. Alizadeh, D.A. Hills, P.F.P de Matos, D. Nowell, M.J. Pavier, R.J. Paynter, D.J. Smith, and S. Simandjuntak. A comparison of two and three-dimensional analyses of fatigue crack closure. *International Journal of Fatigue*, 29(2):222-231,2007

[14] R.C. McClung and H. Sehitoglu. Closure behavior of small cracks under high strain fatigue histories. In J.C. Newman and Jr. W. Elber, editors, *Mechanics of Fatigue Crack Closure, ASTM STP 982*, pages 279-299. American Society for Testing and Materials, 1988

[15] P.L. Lalor and H.Sehitoglu. Fatigue crack closure outside a small-scale yielding regime. In J.C. Newman and Jr. W. Elber, editors, *Mechanics of Fatigue Crack Closure, ASTM STP 982*, American Society for Testing and Materials, 1988

[16] C.F.Shih. Estimates for strain hardening materials in antiplane shear using fully plastic solutions. *Mechanics of Fatigue Crack Growth, ASTM STP*, 590:3-26,1976.

[17] Fully plastic solutions and large scale yielding estimates for plane stress crack problems. *Journal of Engineering Materials and Technology*, 98:289-95,1976.

[18] Fully plastic solutions and large scale yielding estimates for plane stress crack problems. *Journal of Engineering Materials and Technology*, 98:289-95,1976.

[19] Fatigue Crack Growth and Closure at High Cyclic Strains. *Journal of Engineering Materials and Technology*, 98:289-95,1976.

[20] The consequences of short crack closure on fatigue crack growth under variable amplitude loading. *Fatigue and Fracture of Engineering Materials and Structures*, 14(2/3):205-25,1991.

[21] Fatigue crack closure: From LCF to small scale yielding *International Journal of Fatigue*,2012.

[22] Characterization of fatigue crack growth in intermediate and large scale yielding. *Journal of Engineering Materials and Technology*, 113:15-22,1991.

[23] Elastic-plastic fatigue crack growth. *In Advanced Methods of Fatigue Assessment*, pages 391-481. Springer, 2013.

[24] B Tomkins. *Fatigue crack propogation - an analysis*. Philosophical Magazine, 18(155):1041, 1066 1968.

[25] S. Rabbolini, S. Beretta, S.Foletti and A. Riva. *Short crack propogation in LCF regime at room and high temperature in Q&T rotor steels*. International Journal of Fatigue, vol.75, pp. 10-18, 2015.

[26] S. Rabbolini, S. Beretta, S.Foletti and M.E Cristea. *Crack closure effects during low cycle fatigue propagation in line pipe steel: An analysis with digital image correlation.*

[27] Chen, D.H. and Nisitani,H., *"Analytical and Experimental Study of Crack Closure Behavior Based on an S-Shaped Unloading Curve"*. Mechanics of Fatigue Crack Closure, ASTM STP982, ASTM International, West Conshohocken, PA, 1988, pp. 475-488.

[28] Skorupa, M., Beretta, S., Carboni, M., and Machniewicz, T., *"An Algorithm for Evaluating Crack Closure from Local Compliance Measurements"*. Fatigue Fract. Eng. Mater. Struct, Vol. 25, No.3, 2002, pp.261-273.

[29] M.H. El-Haddad and B. Mukherjee. *Elastic-plastic fracture mechanics analysis of fatigue crack growth*. In C.F. Shih and J.P. Gudas, editors, Elastic-Plastic Fracture: Second Symposium, Volume II - Fracture Resistance Curves and Engineering Applications, ASTM STP 803, pages 689-707. ASTM, 1983.

[30] K. Tanaka, T. Hoshide and M. Nakata. *Elastic-plastic fracture mechanics analysis of fatigue crack growth*. In C.F. Shih and J.P. Gudas, editors, Elastic-Plastic Fracture: Second Symposium, Volume II - Fracture Resistance Curves and Engineering Applications, ASTM STP 803, pages 708-722. ASTM, 1983.

[31] M. Jolles. *Effects of load gradients on applicability of a fatigue crack growth rate-cyclic J relation*. In ASTM STP 868, pages 381-391. ASTM, 1985.

[32] W.H. Peters, W.F. Ranson, M.A. Sutton, T.C. Chu and J. Anderson. *Application of digital correlation methods to rigid body mechanics*. Optical Engineering, 22(6):226738-226738,1983.

[33] T.C. Chu, W.F. Ranson, and M.A. Sutton. *Application of digital-image-correlation techniques to experimental mechanics*. Experimental mechanics, 25(3):232-244,1985.

[34] M.A. Sutton, C. Mingqi, W.H. Peters, Y.J. Chao and S.R. McNeill *Application of an optimized digital correlation method to planar deformation analysis*. Image and Vision Computing, 4(3):143-150,1986.

[35] M.A. Bruck, S.R. McNeill, M.A. Sutton and W.H. Peters Iii. *Digital image correlation using newton-raphson method of partial differential correction*. Experimental Mechanics, 29(3):261-267,1989.

[36] S. Rabbolini *Method for LCF Life predictions in presence of defects*. Doctoral Dissertation, AY 2011-2014- cycle XXVII, Politecnico di Milano.

[37] C. Schweizer, H. Riedel *Simulation of fatigue crack growth under Large Scale Yielding conditions*. Journal of Physics Conference Series, August 2010.

[38] S. Pommier, Ph Bompard *Bauschinger effect of alloys and Plasticity-induced crack closure: a finite element analysis*. Fatigue Fracture Engineering Material Structure 23, 129-139, Blackwell Science Limited.

[39] F. Farukh, L. Zhao, R. Jiang, P. Reed, D. Proprentner and B. Shollock *Fatigue crack growth in a nickel-based superalloy at elevated temperature - experimental studies, viscoplasticity modelling and XFEM*. Mechanics of Advanced MAterials and Modern Processes (2015) 1:2.

[40] A. Standard, "E606-92", *Standard Practise for Strain-Controlled Fatigue Testing.* Annual Book of ASTM Standards, Volume 3, 2004.